

RESEARCH ARTICLE

A nuclear localization signal targets tail-anchored membrane proteins to the inner nuclear envelope in plants

Norman R. Groves¹, Joseph F. McKenna², David E. Evans², Katja Graumann² and Iris Meier^{1,3,*}

ABSTRACT

Protein targeting to the inner nuclear membrane (INM) is one of the least understood protein targeting pathways. INM proteins are important for chromatin organization, nuclear morphology and movement, and meiosis, and have been implicated in human diseases. In opisthokonts, one mechanism for INM targeting is transport factor-mediated trafficking, in which nuclear localization signals (NLSs) function in nuclear import of transmembrane proteins. To explore whether this pathway exists in plants, we fused the SV40 NLS to a plant ER tail-anchored protein and showed that the GFP-tagged fusion protein was significantly enriched at the nuclear envelope (NE) of leaf epidermal cells. Airyscan subdiffraction limited confocal microscopy showed that this protein displays a localization consistent with an INM protein. Nine different monopartite and bipartite NLSs from plants and opisthokonts, fused to a chimeric tail-anchored membrane protein, were all sufficient for NE enrichment, and both monopartite and bipartite NLSs were sufficient for trafficking to the INM. Tolerance for different linker lengths and protein conformations suggests that INM trafficking rules might differ from those in opisthokonts. The INM proteins developed here can be used to target new functionalities to the plant nuclear periphery.

This article has an associated First Person interview with the first author of the paper.

KEY WORDS: Protein trafficking, Tail-anchored protein, Nuclear localization signal, Plant, Inner nuclear membrane

INTRODUCTION

The nuclear envelope (NE) is a dual membrane system that encloses the chromatin and separates it from the cytoplasmic environment. The NE is composed of the inner nuclear membrane (INM) and outer nuclear membrane (ONM), and the two membranes are continuous at the sites of nuclear pore complexes. The endoplasmic reticulum (ER) is continuous with the ONM, and the INM and ONM have distinct protein complements. The proteins of the NE have been implicated in a variety of roles, and specifically the INM protein complement plays important roles for both the nucleus and the organism as a whole (Meier et al., 2017).

Known INM proteins in animals and yeast have roles in nuclear movement, nuclear anchoring, chromatin tethering, transcriptional

regulation and mechanotransduction (Starr and Fridolfsson, 2010; Rothballer et al., 2013; Barton et al., 2015; Nikolakaki et al., 2017). Mutations in INM and INM-associated proteins are associated with a variety of human genetic diseases, collectively known as nuclear laminopathies (Janin et al., 2017). In addition, proteomic studies have revealed more than 100 novel nuclear envelope transmembrane proteins (NETs) and show that the nuclear envelope proteome differs significantly between tissues (Korfali et al., 2012; de Las Heras et al., 2013).


An important question in protein trafficking is how INM proteins reach their target destination and what factors lead to their specific accumulation at the INM. Soluble nuclear proteins enter the nucleus by active or passive transport through nuclear pores. Nuclear pore complexes (NPCs) are large protein complexes present at the sites of INM–ONM junctions that are anchored to the pore membrane through transmembrane nucleoporins (Mitchell et al., 2010; Grossman et al., 2012; Kim et al., 2018). The central channel of the NPC contains a phenylalanine–glycine (FG)-rich meshwork that serves as a size exclusion barrier to the import of soluble proteins above 40–60 kDa (Lyman et al., 2002; Patel et al., 2007). Cargo larger than 60 kDa passively enters the nucleus at a vastly decreased rate (Patel et al., 2007; Wang and Brattain, 2007; Popken et al., 2015). Active soluble protein import through the central channel of the nuclear pore involves the binding of proteins that contain a nuclear localization signal (NLS) to nuclear transport receptors called karyopherins (Lange et al., 2007; Soniat and Chook, 2015).

In animals and yeast, protein trafficking to the INM is currently described by two predominant models (reviewed in Katta et al., 2014). The diffusion-retention model states that membrane proteins are first inserted into the ER membrane, either co- or post-translationally. Once inserted, the proteins diffuse between the ER, ONM and INM, only retained at a compartment through protein–protein interaction (Powell and Burke, 1990; Smith and Blobel, 1993; Soullam and Worman, 1993). Extraluminal domains of proteins trafficking to the INM must be small enough to pass through the peripheral channel of the nuclear pore, which provides a physical limit to protein passage (Boni et al., 2015; Ungricht et al., 2015). Increasing the extraluminal domains of INM proteins above 60 kDa decreases NE localization of INM proteins, and the stringency of this size exclusion decreases in nucleoporin mutants (Boni et al., 2015; Ungricht et al., 2015).

In the transport factor-mediated model, a membrane protein containing a nuclear localization signal (NLS) is bound by karyopherins, and trafficking through the nuclear pore by active transport allows for accumulation at the INM. Many INM proteins contain NLSs, and deletion mutants lacking an NLS predominantly localize to the ONM and ER (King et al., 2006; Turgay et al., 2010). Fragments of the *S. cerevisiae* INM LEM domain protein Heh2 containing a NLS are enriched tenfold at the NE over a fragment lacking an NLS (Meinema et al., 2011). In the case of the INM protein SUN2, many signals play a role in trafficking to the INM, including an

¹Department of Molecular Genetics, The Ohio State University, Columbus, OH 43210, USA. ²Department of Biological and Medical Sciences, Oxford Brookes, Oxford OX3 0BP, UK. ³Center for RNA Biology, The Ohio State University, Columbus, OH 43210, USA.

*Author for correspondence (meier.56@osu.edu)

 N.R.G., 0000-0002-6629-7797; J.F.M., 0000-0003-4838-6048; I.M., 0000-0002-4141-5400

NLS, an INM sorting motif and the NE luminal SUN domain (Turgay et al., 2010).

In plants, the nuclear envelope proteome appears to diverge significantly from animals and yeast (Poulet et al., 2017; Meier et al., 2017). SUN proteins are conserved in plants, but no other opisthokont INM proteins have recognizable homologs in plants (Graumann et al., 2010, 2014). Similar to mammalian SUN, *Arabidopsis thaliana* SUN1 and SUN2 require an NLS-containing N-terminal domain for localization to the INM (Graumann et al., 2010). An N-terminal 238-amino-acid fragment of mammalian lamin B receptor (LBR) is targeted to the nuclear envelope in plants and the lamin-binding domain is required for this process, suggesting that LBR contains import features recognized in plants (Irons et al., 2003; Graumann et al., 2007). ONM-localized animal KASH proteins lack homologs in plants, but structurally distinct plant KASH proteins have recently been identified (Zhou et al., 2012, 2014). Additionally, plants lack a nuclear lamina, although plant lamin-like proteins have been reported (Dittmer et al., 2007; Wang et al., 2013; Goto et al., 2014). Aside from these few examples, the plant NE is still largely a black box.

In this study, we sought to determine whether an NLS-dependent pathway for INM trafficking exists in plants with the dual goal of investigating the process of plant INM protein trafficking and to design tools to deliver proteins to this cellular compartment. To this end, we tested whether addition of an NLS to a tail-anchored ER membrane protein is sufficient to redirect it to the NE. Subsequently, fragments of the yeast INM protein Heh2 containing the bipartite NLS were tested for enrichment at the plant NE. Chimeric ER membrane proteins were generated to test whether a variety of NLSs were sufficient for NE enrichment and whether there is a minimum or maximum distance between the NLS and transmembrane domain. Airyscan confocal microscopy was utilized to elucidate whether NLS-fused membrane proteins access the INM (Huff, 2015; Korobchevskaya et al., 2017). Our study provides the first evidence that an NLS-dependent pathway exists in plants, and illustrates that in plants this pathway to the INM is tolerant to different NLSs and protein structures.

RESULTS

Addition of an NLS is sufficient to enrich a plant ER membrane protein at the NE

We first sought to determine whether an endogenous ER membrane protein could be redirected to the nuclear envelope (NE) through fusion with a nuclear localization signal (NLS). For this purpose, the *Arabidopsis* 89 kDa ER tail-anchored coiled-coil protein PAMP-INDUCED COILED-COIL LIKE (PICL; UniProt F4I8Q1) was selected (Venkatakrishnan et al., 2013). The SV40 T-antigen NLS was N-terminally fused to the cytoplasmic domain of PICL (NLS-PICL) (Kalderon et al., 1984). Knowing that the luminal tail domain of the plant KASH protein WIP1 is required for both its interaction with the INM protein SUN1 and enrichment at the NE, we used this SUN-interacting tail (SIT) as a control for NE retention (Zhou et al., 2012). The SIT from WIP1 was fused to the ER luminal C-terminus of PICL to generate PICL-SIT (Fig. 1A). NLS-PICL-SIT, a PICL chimera containing the SV40 NLS and WIP1 SIT, was also generated. N-terminal GFP fusions of each PICL chimera protein were generated, and were transiently expressed under control of the Cauliflower mosaic virus 35S promoter (35S) in *Nicotiana benthamiana* leaf epidermal cells. GFP-PICL was located at the perinuclear ER, the NE and the cortical ER, as described previously (Venkatakrishnan et al., 2013) (Fig. 1B). NLS-fused PICL was enriched at the NE, while a concomitant reduction of ER signal was observed. The signal distribution of PICL-SIT and NLS-PICL-SIT was similar to that of NLS-PICL.

To quantify the signal distribution between NE and cortical ER, a nuclear localization index (NLI) of each PICL variant was calculated, as described previously (Zhou et al., 2012). In brief, the GFP fluorescence intensity was measured along randomly drawn lines crossing the NE and high-intensity GFP signal close to the plasma membrane (representing cortical ER, compare Fig. 1B ‘cross section’ and ‘cortex’) in images representing nuclear cross sections (Fig. S1). The two highest fluorescent signals each at the NE and ER were then used to calculate the ratio $[NLI=(N_1+N_2)/(Cyt_1+Cyt_2)]$. This analysis showed that NLS-PICL was significantly enriched at the NE compared to PICL (Fig. 1C). The NLI of NLS-PICL was indistinguishable from that of PICL-SIT. Combining the two motifs further increased enrichment of the fusion protein at the NE. To validate this approach, we showed that our quantification method remains robust for the range of expression levels that would be expected in a transient transfection protocol (Fig. S1D–F).

An NLS-containing yeast INM protein fragment is enriched at the NE

A fragment of the yeast INM protein Heh2 containing an NLS and single transmembrane domain (TMD) has been previously reported to be enriched at the NE in *Saccharomyces cerevisiae*, compared to the same fragment lacking an NLS (Meinema et al., 2011; Kralt et al., 2015). To test whether yeast Heh2 can access the plant INM and whether the reported combination of NLS, linker and TMD are also sufficient in plants, we amplified Heh2, Heh2-L-TM, and Heh2L-TM, as previously described (Fig. 2A; Meinema et al., 2011). Each Heh2 variant was N-terminally tagged with GFP, and transiently expressed in *N. benthamiana* leaf epidermal cells under the control of the 35S promoter. The full-length Heh2 protein, as well as the fragment lacking the NLS (Heh2L-TM), were moderately enriched at the NE (Fig. 2B,D,E). Heh2NLS-L-TM was enriched at the NE, but large aggregates in the nucleus were also consistently observed (Fig. 2C,E). Under the assumption of topologically correct insertion of Heh2 and Heh2 fragments in the membrane, these data suggest that the Heh2NLS-L-TM fragment of Heh2 does have features that bring it to the plant NE, but that this is less the case when it is part of full-length Heh2, suggesting that yeast and plants recognize and target this protein in different ways.

Monopartite and bipartite NLSs are sufficient for NLS-mediated NE enrichment

To generate a non-endogenous ER membrane protein, the intrinsically disordered linker from Heh2 was fused to the WIP1 TMD to generate Heh2Linker-TMD (Fig. 3A,B). This chimeric tail-anchored protein localized to the NE and ER in a nuclear cross section of transiently transformed *N. benthamiana* leaf epidermal cells (Fig. 3C,D). Heh2Linker-TMD colocalizes with an ER marker, calnexin-mCherry (Fig. 3E; Irons et al., 2003). N-terminal fusion of the SV40 NLS to the chimeric membrane protein Heh2Linker-TMD resulted in a significant enrichment at the NE (Fig. 3C,D).

The bipartite NLS of yeast Heh2 (and Heh1) strongly associates with the minor NLS-binding pocket of importin α in a different manner from classical NLS binding, and this difference likely plays a role in making the Heh2 NLS more effective for membrane protein nuclear import in yeast (Kralt et al., 2015; Lokareddy et al., 2015). The above data suggest that re-targeting from the ER to the NE in *N. benthamiana* functions similarly when driven by the bipartite Heh2 NLS and by the classical SV40 NLS (compare Fig. 2 and Fig. 3). Therefore, we systematically tested a variety of confirmed and predicted NLSs in the context of Heh2Linker-TMD. Five monopartite NLSs were selected, representing different structural

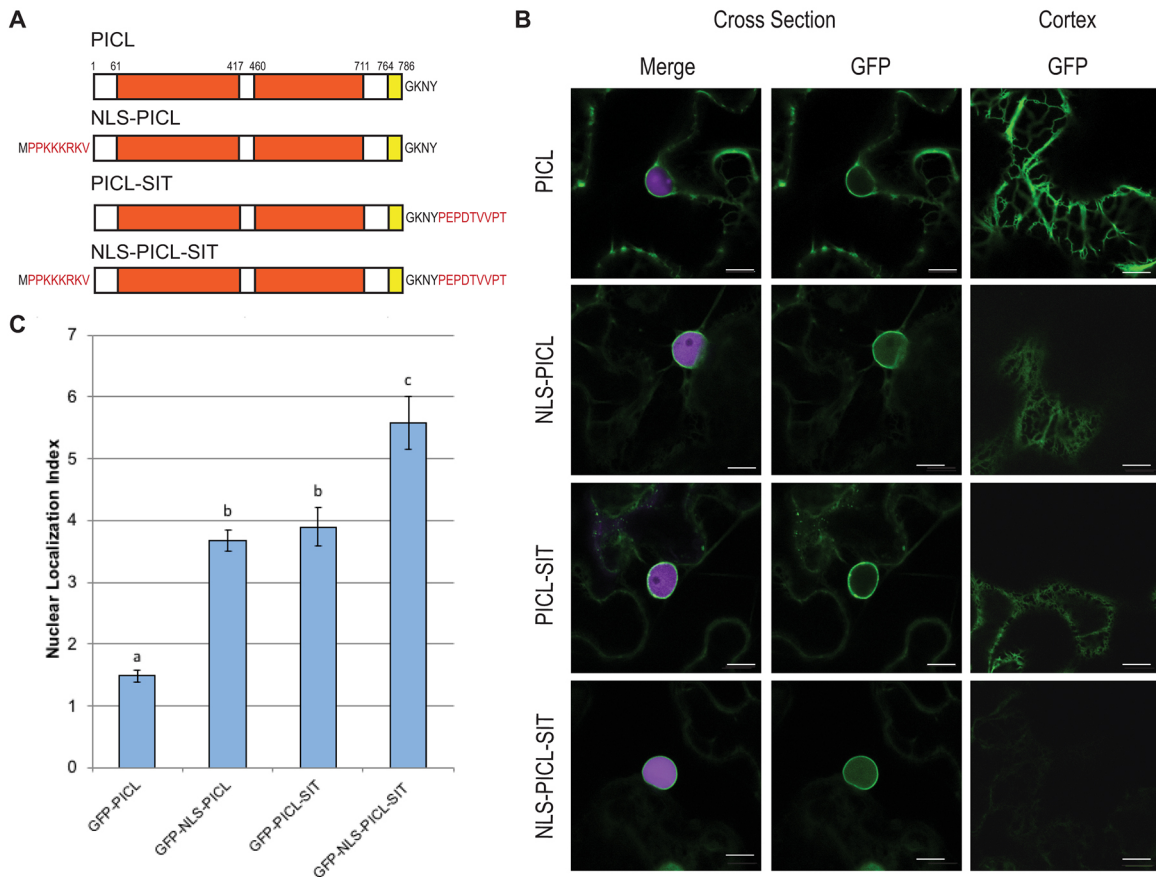


Fig. 1. An NLS is sufficient to enrich an ER tail-anchored protein at the nuclear envelope. (A) The domain structure of the *Arabidopsis* tail-anchored ER membrane protein PICL. PICL contains a single C-terminal transmembrane domain (yellow) and two coiled-coil domains (orange). The SV40 T-antigen NLS was fused to the N-terminus of PICL in NLS-PICL and NLS-PICL-SIT. The SIT of the *Arabidopsis* KASH protein WIP1 was fused to the C-terminus of PICL in PICL-SIT and NLS-PICL-SIT. This is indicated in red single amino acid code. The terminal four amino acids of PICL are indicated in black. (B) GFP was fused to the N-terminus of PICL or PICL chimeric proteins and transiently co-expressed with a nuclear marker (H2B-mCherry; purple) in *N. benthamiana* leaf epidermal cells. GFP fluorescence in nuclear cross sections is shown with (Merge) and without (GFP) mCherry fluorescence in cross sections of the nucleus. The GFP signal in cortical layer (Cortex) of same cell shown as shown in cross section. Scale bars: 10 μ m. (C) Relative NE enrichment of PICL and PICL chimeric proteins was determined by calculating the average NLI (see Fig. S1). Statistical significance was calculated using Student's *t*-test, and groups that are statistically different from each other ($P < 0.001$) are denoted by different lowercase letters. Error bars denote the s.e.m.

classes of monopartite NLS previously reported (CL1–CL5, see Table S1) (Kosugi et al., 2009). Two of the five monopartite sequences were previously shown to function as an NLS, while the remaining three were hypothetical NLSs tested for their ability to bind importin α (Kalderon et al., 1984; Dang and Lee, 1988; Kosugi et al., 2009). One of these predicted NLSs, denoted class 5 (CL5), has been shown to only bind a plant importin α (Kosugi et al., 2009). Four bipartite NLSs were selected for testing, including the well-characterized nucleoplasmin NLS (Robbins et al., 1991). Three of the bipartite NLSs originate from plant species (Table S1; Varagona et al., 1992; Graumann et al., 2010). Two of the plant bipartite NLSs, SUN1 NLS and SUN2 NLS, are predicted NLSs from the *Arabidopsis* INM proteins SUN1 and SUN2 (Graumann et al., 2010). The third plant bipartite NLS originates from the maize transcription factor Opaque2 (Opq2) (Varagona et al., 1992).

First, the selected NLSs were tested for their ability to function in soluble protein import. Each NLS was fused to a soluble cargo, GFP-GUS (β -glucuronidase, UniProt P05804; Jefferson et al., 1987). Each soluble cargo was transiently expressed in *N. benthamiana* under the control of the 35S promoter (Fig. S2). GFP-GUS lacking an NLS was excluded from the nucleus. All tested NLSs were sufficient for nuclear localization of NLS-GFP-

GUS, with the exception of those derived from *Arabidopsis* SUN1 and SUN2 (Fig. S2). NLSs from SUN1 and SUN2 in both human cell lines and *Arabidopsis* are necessary for efficient NE and INM localization, but sufficiency has never been tested (Graumann et al., 2010; Turgay et al., 2010). As SUN1 and SUN2 are the only NLSs that originated from INM proteins, they were nevertheless included in the further experiments (Graumann et al., 2010).

Each of the nine NLSs were fused to Heh2Linker-TMD to generate different NLS-Heh2Linker-TMD fusion proteins (Fig. 4C). GFP fusions of the nine varieties of NLS-Heh2Linker-TMD were transiently expressed in *N. benthamiana* and subcellular localization was observed. Each of the monopartite NLSs tested was sufficient to enrich the chimeric membrane protein at the NE (Fig. 4A). Similarly, each bipartite NLS was sufficient to enrich NLS-Heh2Linker-TMD at the NE, including the NLSs of *Arabidopsis* SUN1 and SUN2 that had not shown nuclear import activity for the soluble GFP-GUS protein (Fig. 4B). NLI calculation showed all nine NLSs were sufficient to enrich Heh2Linker-TMD to a statistically significant degree at the NE. However, there were quantitative differences observed between the NLSs, with the SUN2 NLS leading to the least NE enrichment and the Opq2 NLS to the greatest enrichment (Fig. 4D). In addition to NE enrichment, some

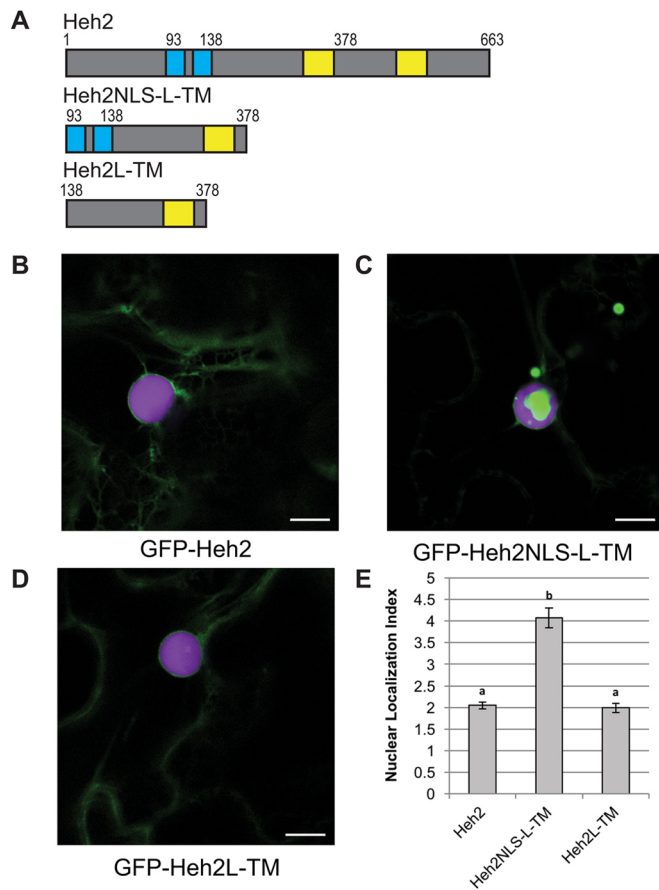


Fig. 2. Subcellular localization of *S. cerevisiae* Heh2 and Heh2 fragments in *N. benthamiana*. (A) The domain structure of the Heh2 fragments previously tested for NE enrichment in *S. cerevisiae*. TMDs (yellow) and NLSs (blue) are denoted. Numbers indicate amino acid positions for the borders of NLSs (beginning of the first blue box and end of the second blue box) and the end of the Heh2L-TM fragment indicated in Meinema et al. (2011) (position 378 as depicted in the Heh2L-TM fragment). (B–D) GFP fusions of full-length Heh2 and Heh2 fragments were transiently expressed in *N. benthamiana* leaf epidermal cells. H2B-mCherry was co-expressed as a nuclear marker (purple). Scale bars: 10 μ m. (E) The NLI of Heh2 fragments was calculated as in Fig. S1. Statistical significance was calculated using Student's *t*-test, and groups that are statistically different from each other ($P < 0.001$) are denoted by different lowercase letters. Error bars denote the s.e.m.; $n = 20$ cells.

NLS sequences resulted in the formation of nuclear deformations and invaginations (Fig. S3), which has been previously reported for the overexpression of NE-associated plant proteins (Goto et al., 2014). At the cell cortex, Heh2Linker-TMD and all NLS-Heh2Linker-TMD variants were located at the cortical ER, indicating that the majority of the cytoplasmic fusion proteins are associated with the membrane (Fig. S4).

NLS-mediated NE enrichment is tolerant to different protein conformations between the NLS and TMD

To determine whether NLS-mediated NE enrichment is limited to proteins containing an intrinsically disordered linker, chimeric membrane proteins were designed that contained a coiled-coil domain fused to a TMD. The coiled-coil domain from WIP1 (WIP1CC, amino acids 323–446, Fig. 3A) was fused to the WIP1 TMD to generate WIP1CC-TMD (Fig. 5A; Zhou et al., 2012). WIP1CC-TMD was moderately enriched at the NE compared to Heh2Linker-TMD (Fig. 5B,C). The five monopartite NLSs previously tested were N-terminally fused to generate NLS-

WIP1CC-TMD varieties. All NLS-WIP1CC-TMD varieties were enriched at the NE, compared to WIP1CC-TMD (Fig. 5B,C). The combination of the SV40 NLS and WIP1CC-TMD resulted in nuclear aggregates similar to those observed with Heh2 (compare Fig. 2C and Fig. 5B). NLS-WIP1CC-TMD NE enrichment was not significantly different from NLS-Heh2Linker-TMD for the SV40 NLS and CL4 NLS, and was reduced compared to NLS-Heh2Linker-TMD for the cMyc NLS, CL3 NLS and CL5 NLS (Fig. 5B,C). These data indicate that both disordered and ordered domains can be tolerated for NLS-mediated NE enrichment. However, an intrinsically disordered region appears to be preferable.

We additionally tested whether the position of the NLS relative to GFP affected NE enrichment. NLS-GFP-Heh2Linker-TMD varieties were generated for the SV40 NLS and CL3 NLS monopartite NLSs, and compared to their GFP-NLS-Heh2Linker-TMD counterparts (Fig. S5A). All NLS-fused proteins were enriched at the NE compared to GFP-Heh2Linker-TMD (Fig. S5B,C). NLS position had no effect on NE enrichment of the CL3 NLS, but a difference in NE enrichment was observed for the SV40 NLS (Fig. S5C).

NLS-mediated NE enrichment is tolerant to limited space between NLS and TMD

To determine whether a minimal distance between NLS and TMD exists for the NLS-mediated NE enrichment, increasingly small fragments of the Heh2Linker were generated. The full length Heh2Linker is 145 amino acids in length, and 100, 50 and 10 amino acid fragments were amplified from the Heh2Linker N-terminus and fused to the WIP1 TMD (Meinema et al., 2011). A monopartite NLS (SV40 NLS) or bipartite NLS (Opq2 NLS) was fused to the short linkers to generate NLS-fused chimeric membrane proteins of variable length (Fig. 6A). A *Hind*III restriction site was introduced at the 3' end of the Heh2Linker variants to facilitate further manipulation of the size and structure of these proteins. All NLS-fused short linker variants were localized to the NE and cortical ER (Fig. 6B,D; Fig. S6B). All NLS-fused short linker variants were enriched at the NE compared to Heh2Linker-TMD, with the exception of the SV40 NLS-fused 100 amino acid variant (Fig. 6C,E). The SV40NLS-Link100 variant localized to the NE and ER, with punctate structures lining the ER (Fig. 6B; Fig. S6B). Both NLS-fused 10 amino acid variants had an increased NE enrichment compared to the other short linker variants, along with an increased diffuse nuclear accumulation (Fig. 6B,D; Fig. S6A). Taken together, these data indicate that NLS-mediated NE enrichment is tolerant to distances as short as 10 amino acids between an NLS and TMD.

NLS-mediated NE enrichment of PICL suggests that this pathway is tolerant to extralumenal domains of up to 115 kDa. To further explore size constraints in the context of the disordered linker, the full length Heh2 intrinsically disordered linker and Heh2Linker truncations were combined to increase the distance between NLS and TMD (Fig. S7A). SV40 NLS-fused varieties of these chimeric membrane proteins were transiently expressed in *N. benthamiana*, and similar to their smaller counterparts, were enriched at the NE (Fig. S7B,C). Thus, increasing the extralumenal domain above 60 kDa has no major effect on NE enrichment (Fig. S7C).

NLS-fused membrane proteins access the INM

Differentiating between the ONM and INM is a challenging experimental question in all systems (King et al., 2006; Capoen et al., 2011; Zuleger et al., 2011; Mudumbi et al., 2016; Smoyer et al., 2016). Here, we tested whether Airyscan subdiffraction

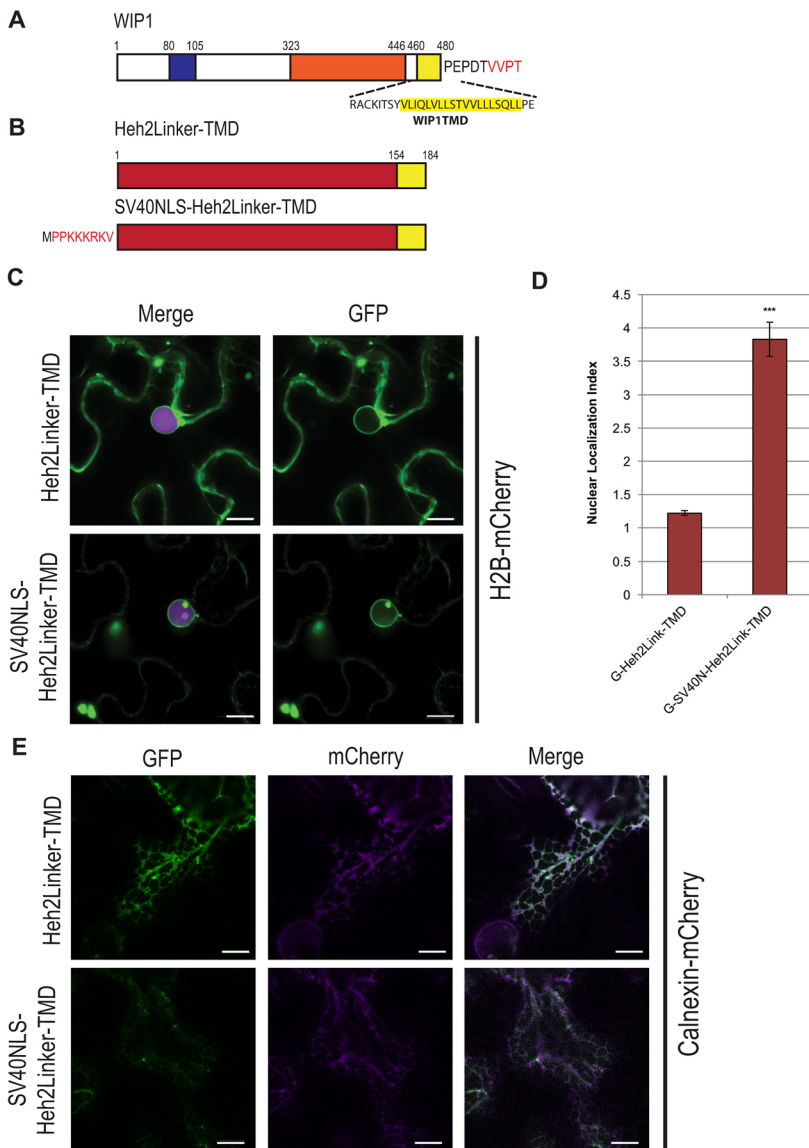


Fig. 3. Addition of an NLS is sufficient to target a chimeric membrane protein to the NE. (A) The domain structure of the ONM KASH protein WIP1. The NLS (blue), coiled-coil domain (orange) and TMD (yellow) are shown. The 4-amino-acid KASH tail is colored in red. The sequence of the transmembrane fragment used in B is detailed. (B) The domain structure of the chimeric ER membrane protein Heh2Linker-TMD. Heh2linker-TMD was generated by fusing the linker domain of the *S. cerevisiae* inner nuclear membrane protein Heh2 (amino acids 138–283, see A) to the TMD of the *Arabidopsis* KASH protein WIP1 (Zhou et al., 2012). The SV40 T-antigen NLS was fused to the N-terminus of Heh2Linker-TMD, resulting in SV40NLS-Heh2Linker-TMD. (C) Chimeric membrane proteins were N-terminally fused to GFP and transiently co-expressed with H2B-mCherry (purple) in *N. benthamiana* leaf epidermal cells. Scale bars: 10 μ m. (D) NLI were calculated for GFP-Heh2Linker-TMD (G-Heh2Link-TMD) and GFP-SV40NLS-Heh2Linker-TMD (G-SV40N-Heh2Link-TMD) to determine relative NE enrichment (see Fig. S1). *** $P < 0.001$ (Student's *t*-test). Error bars denote s.e.m.; $n = 40$ –80 cells. (E) Images of the localization of GFP fusions detailed in B (GFP) were co-expressed with an ER marker, calnexin-RFP (RFP) to determine if chimeric membrane proteins localize to the ER.

limited imaging can be used to determine whether the NLS-fused proteins investigated in this study access the INM. Airyscan imaging allows a resolution of 140 nm to be reached and can readily be performed on live samples (Huff, 2015; Korobchevskaya et al., 2017). To determine whether fluorescent signals from INM and ONM markers can be separated using this method, we used the ER-localized fusion protein calnexin-mCherry as a marker of the ONM–ER continuum (Liu et al., 2017). We then used markers for the ONM (WIP1) (Xu et al., 2007), INM (SUN2) (Graumann et al., 2010) and nuclear periphery (CRWN1) (Dittmer et al., 2007) fused to GFP, CFP and YFP, respectively, and performed colocalization analyses (Fig. 7A–C). Line profiles were generated from representative images to demonstrate whether peak fluorescence of a marker was separated from the ONM/ER marker calnexin-mCherry. As seen in Fig. 7B,C, there was a high degree of colocalization between GFP-WIP1 and calnexin-mCherry, consistent with WIP1 being an ONM protein. However, the degree of colocalization between SUN2 and calnexin-mCherry is statistically significantly decreased compared to WIP1. As SUN2 has been demonstrated to be an INM protein, this data establishes that Airyscan imaging can differentiate between ONM and INM proteins. In addition, we used

the nuclear periphery marker CRWN1-YFP, further separated from the ONM/ER than SUN2. When co-expressed with calnexin-mCherry, a further decrease in Pearson's correlation coefficient was observed compared to SUN2 (Fig. 7C).

To further support the use of Airyscan subdiffraction limited imaging to separate INM and ONM fluorescence, we determined the ratio of the INM:ONM fluorescence for control datasets (Fig. S8A,B). By subtracting the ONM calnexin-mCherry channel from the control marker channels (WIP1, SUN2 and CRWN1) and then determining the ratio between the maximum intensity of the subtracted channel and the maximum intensity of the unsubtracted WIP1, SUN2, and CRWN1 channels calnexin, we determined the ratio of the INM:ONM fluorescence. When we compared control proteins for the ONM (WIP1), the INM (SUN2) and the nuclear periphery (CRWN1), we saw the same pattern of statistical significance seen with colocalization analysis (Fig. 7). WIP1 showed a low ratio of INM:ONM correlating with its use as an ONM marker, SUN2 showed a higher ratio of max INM to ONM signal, and the nuclear periphery marker (CRWN1) showed the highest ratio of INM:ONM fluorescence. Furthermore, the values for the INM marker were also statistically significantly different

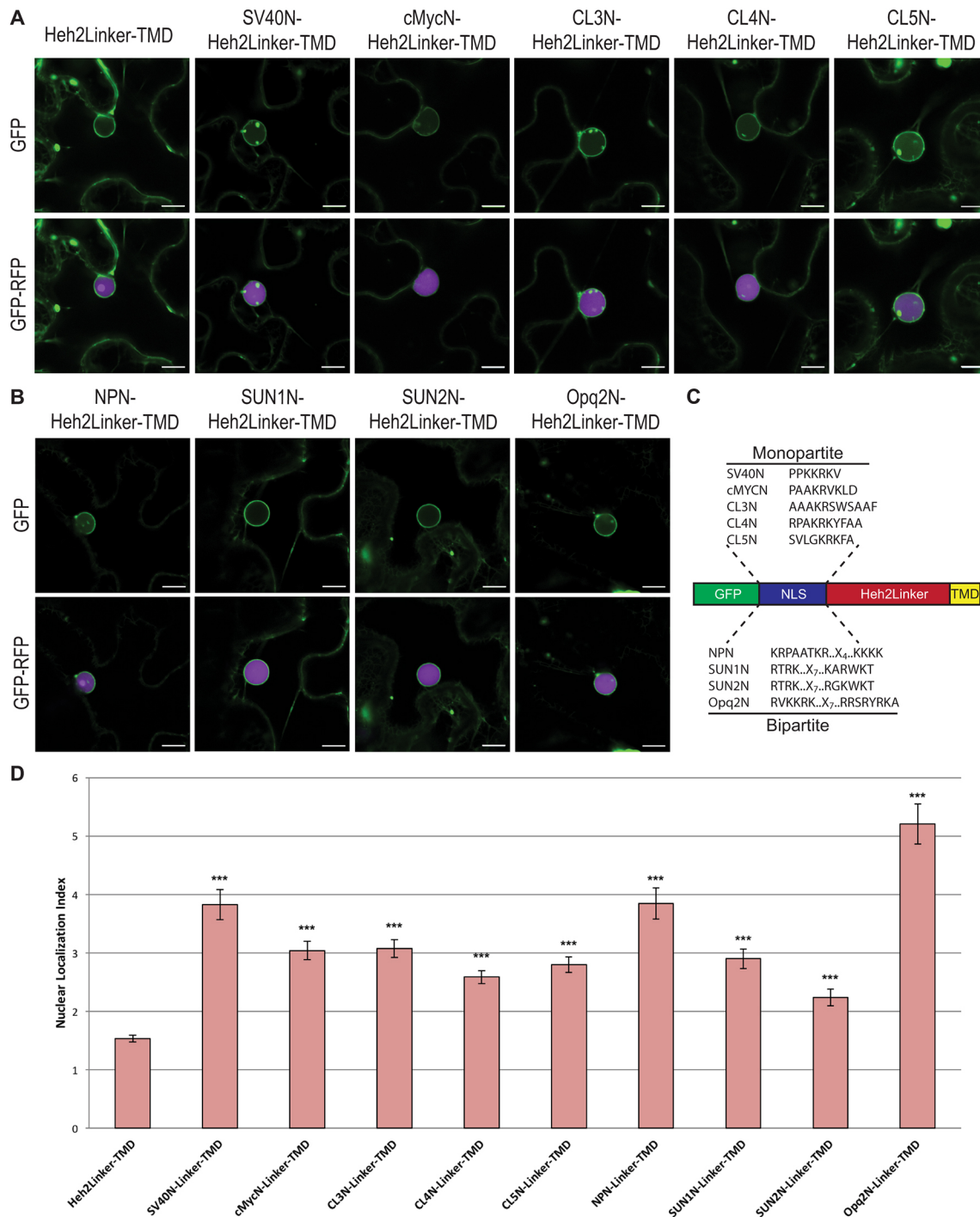
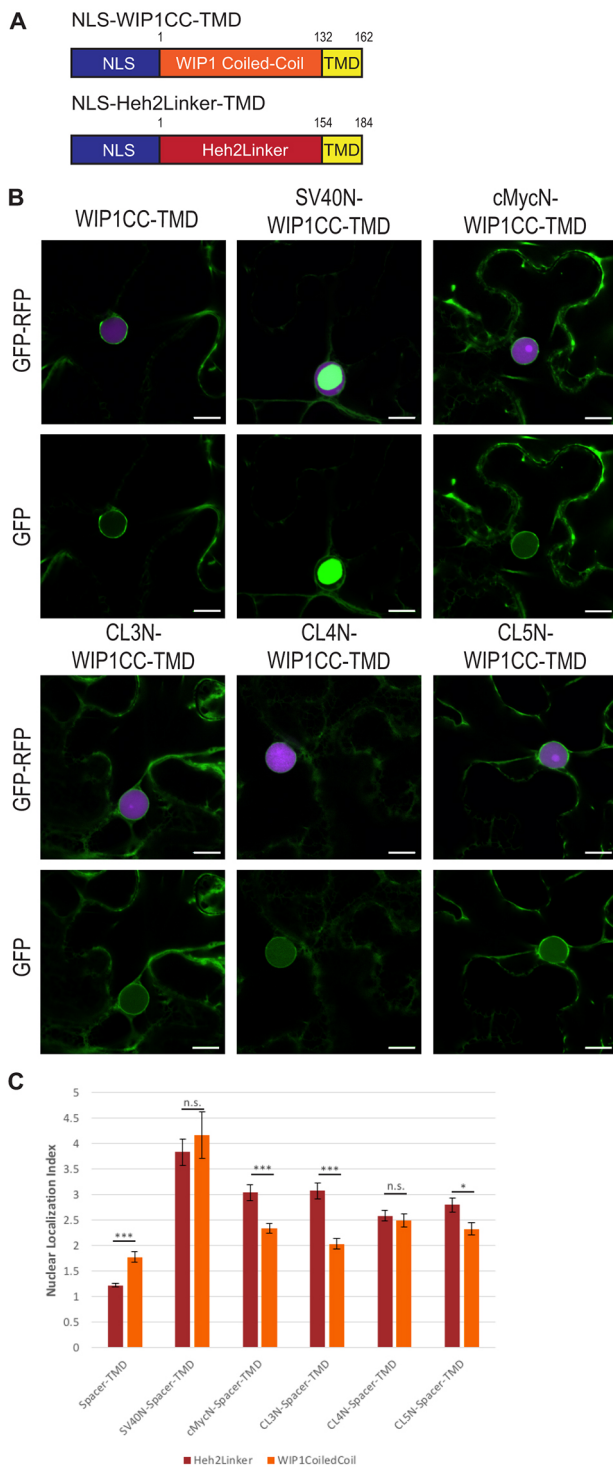


Fig. 4. Monopartite and bipartite NLSs are sufficient to enrich membrane proteins at the nuclear envelope. (A) The chimeric membrane protein, Heh2Linker-TMD was N-terminally fused with one of the five indicated monopartite NLSs. The resulting proteins were N-terminally tagged with GFP and transiently expressed in *N. benthamiana* leaf epidermal cells alongside H2B-mCherry as a nuclear marker (purple). Scale bars: 10 μ m. (B) One of four indicated bipartite NLSs were N-terminally fused to Heh2Linker-TMD. GFP fusions of bipartite NLS-Heh2Linker-TMD were transiently expressed as described in A. Scale bars: 10 μ m. (C) Domain organization and sequences of NLS used in the experiments shown in A and B. X indicates amino acids not a part of a basic cluster. See Table S1 for full names and sequences of NLSs. (D) Average NLIs of cells imaged as shown in A and B, and analyzed as shown in Fig. S1. *** P <0.001 (Student's t -test). Error bars are s.e.m.; n >38 cells for all chimeric membrane proteins.

from the nuclear periphery marker, as we had previously demonstrated (Fig. 7). Together, this analysis shows that when combined with large sample sizes, Airyscan microscopy can separate different compartments of the nuclear periphery.

Next, we tested the PICL-based fusion proteins shown in Fig. 1. Fig. 8A shows the theoretically predicted predominant localization

of the different fusion proteins. PICL shows a high correlation with the ONM/ER marker, while inclusion of the SV40 NLS (GFP-NLS-PICL) resulted in a significant decrease in colocalization with calnexin-mCherry (Fig. 8B,C). Inclusion of the SUN-interacting tail (SIT)-sequence produces a non-significant decrease in PICL-SIT colocalization with the ONM/ER when compared to that of PICL.



Therefore, the NLS enables INM localization while, as expected, the SIT domain does not. In addition, inclusion of both the NLS and SIT sequence (NLS-PICL-SIT), produces a protein that is less colocalized with the ER/ONM marker than PICL, but not as much as NLS-PICL, possibly indicative of a competition between the two signals (Fig. 8B,C).

In addition to NLS-PICL, we tested the chimeric membrane proteins composed of Heh2Link-TMD and fusions with two representative NLSs (CL3N-Heh2Link-TMD and Opq2N-Heh2Link-TMD, Fig. 8D,E). Inclusion of either the monopartite (CL3 NLS) or the bipartite (Opq2 NLS) NLS sequence was

Fig. 5. NLS-TMD-driven NE enrichment is tolerant of different linker structures, but qualitative differences exist. (A) The domain structure of the chimeric membrane proteins NLS-Heh2Linker-TMD and NLS-WIP1CC-TMD. NLS-Heh2Linker-TMD was generated as described in Fig. 4A. NLS-WIP1CC-TMD was generated by fusing the coiled-coil domain (amino acids 323–446) of the *Arabidopsis* KASH protein WIP1 to the TMD (amino acids 452–482) of the same protein. (B) The indicated monopartite NLSs were N-terminally fused to WIP1CC-TMD to generate NLS-WIP1CC-TMD. N-terminal GFP fusions of NLS-WIP1CC-TMD were transiently co-expressed in *N. benthamiana* leaf epidermal cells with the nuclear marker H2B-mCherry (purple). Scale bars: 10 μ m. (C) The NLI was calculated for WIP1CC-TMD and all five NLS-WIP1CC-TMD chimeric membrane proteins (see Fig. S1). NLIs are shown in comparison to the monopartite NLS-Heh2Linker-TMD data shown in Fig. 4D. * P <0.05; *** P <0.001 (Student's t -test). Error bars are s.e.m.; n >25 nuclei for all WIP1CC-TMD membrane proteins and n >38 cells for all Heh2Linker-TMD membrane proteins.

sufficient to statistically significantly decrease the colocalization between the fusion protein and the ONM/ER marker calnexin-mCherry. Furthermore, CL3N-Heh2Link-TMD had a greater decrease in ONM/ER colocalization and was statistically significantly different from Opq2N-Heh2Link-TMD. This can also be seen from the greater difference in peak line profiles (Fig. 8D). To conclude, we have demonstrated using Airyscan subdiffraction limited microscopy imaging combined with statistical colocalization analysis that the NLS-tagged proteins can access the plant INM.

DISCUSSION

While the role of NLSs in INM protein trafficking has been addressed in animals and yeast, our study is the first to look at direct impact of NLSs on protein trafficking to the NE and INM in plants. Our data show that addition of an NLS is sufficient to concentrate tail-anchored ER membrane proteins at the NE and to provide access to the INM. A variety of NLSs, including monopartite and bipartite NLSs, function in this assay, indicating that, in plants, NLSs can broadly act as signals for INM trafficking.

The NLS-fused membrane proteins studied here are likely passing through the nuclear pore with the help of transport factors rather than by diffusion coupled with retention (Katta et al., 2014). Both accumulation at the NE and access to the INM depend on the presence of an NLS. That the NLS sequence might act in another, unpredicted way (for example as a DNA-binding motif) is unlikely given that nine different NLS sequences all were shown to function in this assay and did so in the context of different protein conformations. The tested proteins thus provide little binding surface that might act in retention, given that the NLS-free equivalents did not accumulate at the NE or reach the INM. Testing of protein mobility through fluorescence recovery after photobleaching (FRAP) revealed that two different NLS-fused chimeric membrane proteins (CL3N-Heh2Linker-TMD and Opq2N-Heh2Linker-TMD) are less mobile at the NE than the chimeric membrane protein without NLS (Heh2linker-TMD) (Fig. S8C–H). This difference in mobility could be due to the different membrane environments at the INM versus the ONM/ER, different protein size and/or conformation, or differences in protein–protein interactions, including the putative karyopherin binding.

The yeast INM protein Heh2 remains the most well studied INM protein from the perspective of trafficking. The Heh2 NLS–importin interaction has been mapped, and the Heh2 bipartite NLS has been determined to be atypical in that it strongly competes off the autoinhibitory IBB domain of importin α (Lokareddy et al., 2015). The Heh2 NLS also works in nuclear import of membrane proteins in mammalian cells, and conversely, the closely related NLS of

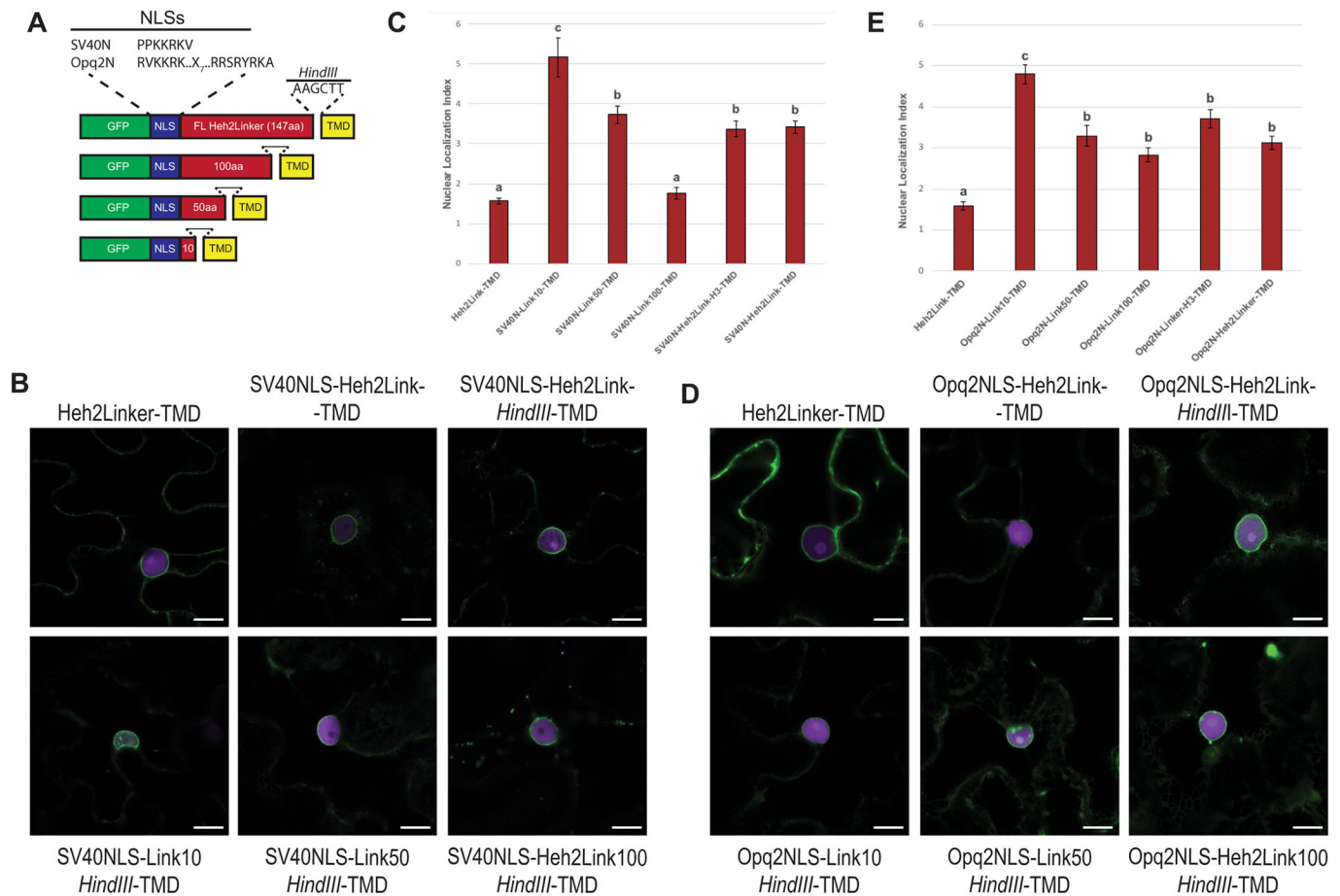


Fig. 6. NLS-mediated NE enrichment is tolerant to short linkers between NLS and TMD. (A) NLSs were N-terminally fused to either the full-length Heh2 linker (Heh2linker), or fragments of 100, 50 or 10 amino acids (Link100, Link50 and Link10). The resulting fragments were expressed in the N-terminal GFP- and C-terminal TMD-fusion vector pK7TMW0WGF2. A *HindIII* restriction site was introduced for further cloning. (B,D) The SV40 NLS or Opq2 NLS was fused to short linker fragments, and the resulting chimeric membrane proteins were N-terminally fused to GFP and transiently co-expressed in *N. benthamiana* leaf epidermal cells with the nuclear marker H2B-mCherry (purple). Scale bars: 10 μ m. (C,E) The NLI was calculated for Heh2Linker-TMD and all NLS-fused short linker chimeric membrane proteins. Statistical significance was calculated using Student's *t*-test, and groups that are statistically different from each other ($P < 0.001$) are denoted by different lowercase letters. Error bars are s.e.m.; $n = 40$ cells for all chimeric membrane proteins.

mammalian POM121 works in yeast. However, none of the other mammalian NLS sequences derived from membrane proteins that were tested worked in yeast, suggesting that, although active import is conserved between yeast and mammals, it is restricted to specific types of NLS (Kralt et al., 2015).

None of the NLSs tested in this study overtly fit the Heh2 NLS archetype. Among the monopartite NLSs tested, the SV40 NLS and cMyc NLS bind to the major binding pocket of importin α , while the class 3 and class 4 NLSs bind to the minor pocket (Kosugi et al., 2009). Among the bipartite NLSs, only the nucleoplasmin NLS has been tested for importin α binding, and binds to both the major and minor pocket (Kosugi et al., 2009). Based on our data, whether an NLS binds to the major binding pocket (e.g. SV40 NLS), minor binding pocket (e.g. CL3 NLS) or both (nucleoplasmin NLS), has no discernable impact on NE enrichment or INM trafficking. It appears that while some NLSs are preferable for directing a membrane protein to the INM, NLSs broadly are sufficient for NE enrichment and trafficking to the INM.

Previous data has indicated that mammalian membrane proteins that accumulate at the INM via diffusion and retention have an upper size limit for extralumenal domains of ~ 60 kDa (Boni et al., 2015; Ungricht et al., 2015). In yeast, this size limit is relaxed to ~ 90 kDa for passive import (Popken et al., 2015). A recent study reported that

membrane proteins imported via transport factors may overcome this size limit, and that proteins with up to 136 kDa extralumenal domain could be actively transported (Laba et al., 2015). The data presented here suggests that an upper size limit, if it exists, may also be more relaxed in plants because GFP-tagged NLS-fused PICL has an extralumenal domain of 115 kDa and because extending the intrinsically disordered region of the NLS-Heh2Linker-TMD chimeric membrane proteins to 297 amino acids also does not meaningfully impact NE enrichment.

The shortest linker between TMD and NLS tested here consisted of 10 amino acids, which still allowed for significant NE accumulation. In yeast, a distance between NLS and TMD below 90 amino acids results in abolishment of NLS-mediated NE enrichment (Meinema et al., 2011, 2013). The shortest linker distance tested in yeast, 37 amino acids, resulted in no observed nuclear accumulation, suggesting a different accommodation of proteins with short linkers between TMD and NLS in plants.

The structure of the nuclear pore complex (NPC) in the green alga *Chlamydomonas reinhardtii* has recently been elucidated (Mosalaganti et al., 2018). While the NPC has been studied in *Arabidopsis* at a genomic level, this is the first structural information of the nuclear pore in the Viridiplantae (Tamura et al., 2010; Tamura and Hara-Nishimura, 2012). While the genes and super structures

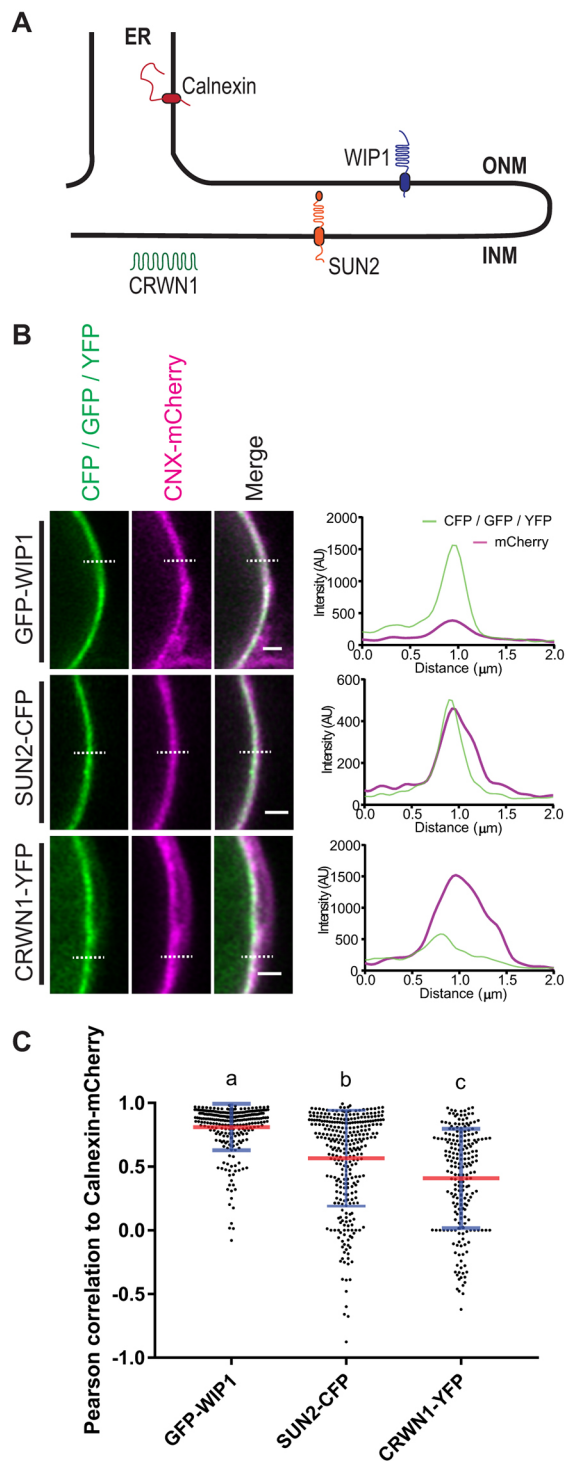


Fig. 7. INM and ONM proteins can be resolved using Airyscan confocal microscopy. (A) Figure illustrating protein localization in the ER, ONM, INM and nuclear periphery. (B) Airyscan subdiffraction limited microscopy was used, with the ER and ONM (calnexin-mCherry) labeled in magenta and marker proteins localized in the ONM (WIP1-GFP), INM (SUN2-CFP) and nuclear periphery (CRWN1-YFP) labeled in green. White dotted lines indicate the area at which line profiles were taken. Line profiles generated over GFP and mCherry images show displacement of peaks between different markers (green) and the ONM (red). Scale bars: 1 μm . (C) Pearson's correlation of marker proteins (WIP1, SUN2 and CRWN1) relative to ONM labeling with calnexin-mCherry demonstrating statistically significant decreases in correlation between ONM and the labeled INM and nuclear periphery when imaged with Airyscan microscopy. A one-way ANOVA statistical test was performed with multiple comparisons, and groups that are statistically different from each other ($P < 0.001$; see Table S2) are denoted by different lowercase letters. In the plots, blue lines indicate error bars showing standard deviation, and red lines show the mean value. A minimum of 35 nuclei were imaged across three experimental repeats with a minimum of 210 areas used for colocalization analysis.

into a lipid bilayer. An alternative pathway for these proteins would be to traffic through the nuclear pore as soluble cargo, and subsequently be inserted into the INM post-translationally. However, several lines of evidence suggest that this hypothetical pathway is not occurring here. First, while all tested NLS sequences were sufficient for NE enrichment, two sequences did not efficiently function in soluble nuclear import (Fig. S2). Interestingly, these are the predicted NLS sequences of *Arabidopsis* SUN1 and SUN2, the only NLSs in this study from known plant INM proteins (Graumann et al., 2010). Specialized importins for INM trafficking have been identified in other systems, leading to the possibility that different sets of importins recognize NLSs in the context of membrane-associated cargoes (Saksena et al., 2006; Liu et al., 2010; Tapley et al., 2011). Currently, dependence of the pathway established here on *Arabidopsis* karyopherins could not be directly tested. There are 10 largely uncharacterized importin α homologs in *Arabidopsis*, in addition to at least seven importin β homologs and one transportin 1 homolog (Merkle, 2011; Tamura and Hara-Nishimura, 2014). As such, determining whether a specialized importin for INM trafficking exists in plants will require further study.

Second, the cytoplasmic fluorescence we observed in nuclear and cortical cross sections is consistent with predominant ER localization for both NLS-fused and non-NLS chimeric membrane proteins (Fig. 4; Fig. S4). While the possibility remains that the proteins could be imported into the nucleus as soluble cargo, the evidence here suggests that the majority of these proteins are membrane associated prior to NPC trafficking. Finally, an increased accumulation of diffuse, nuclear fluorescence was clearly observed when the linker distance between NLS and predicted TMD was shortened to 10 amino acids (Fig. S6). We hypothesize that in this case the close proximity of the NLS to the predicted TMD prevents simultaneous binding of a karyopherin complex to the NLS and an unknown factor – possibly involved in post-translational membrane insertion – to the TMD, resulting in a soluble fraction of the protein being imported into the nucleus.

Post-translational membrane insertion of tail-anchored proteins is not well understood in plants. In yeast, tail-anchored membrane proteins are inserted into the ER membrane post-translationally via the GET pathway (Shao and Hegde, 2011). GET3 is the targeting factor responsible for binding the translated cargo and shuttling it to the ER membrane for reception by GET1/2. *Arabidopsis* has three paralogs of GET3, each located in a different cellular compartment (Xing et al., 2017). GET3a is located in the cytosol and interacts with the other components of the GET pathway, whereas GET3b is

that make up the NPC are largely conserved between humans and *Chlamydomonas*, the diameter of the central channel is larger in *Chlamydomonas* and the *Chlamydomonas* pore is predicted to have the unique feature of significantly larger peripheral channels, which are open to the central channel (Moslaganti et al., 2018). Such a pore structure could potentially accommodate greater variability in the distance between a membrane-inserted TMD and a karyopherin-associated NLS and thus account for the more promiscuous distance requirements observed here.

Our assay does not formally reveal whether the proteins studied here are trafficking through the plant nuclear pore while inserted

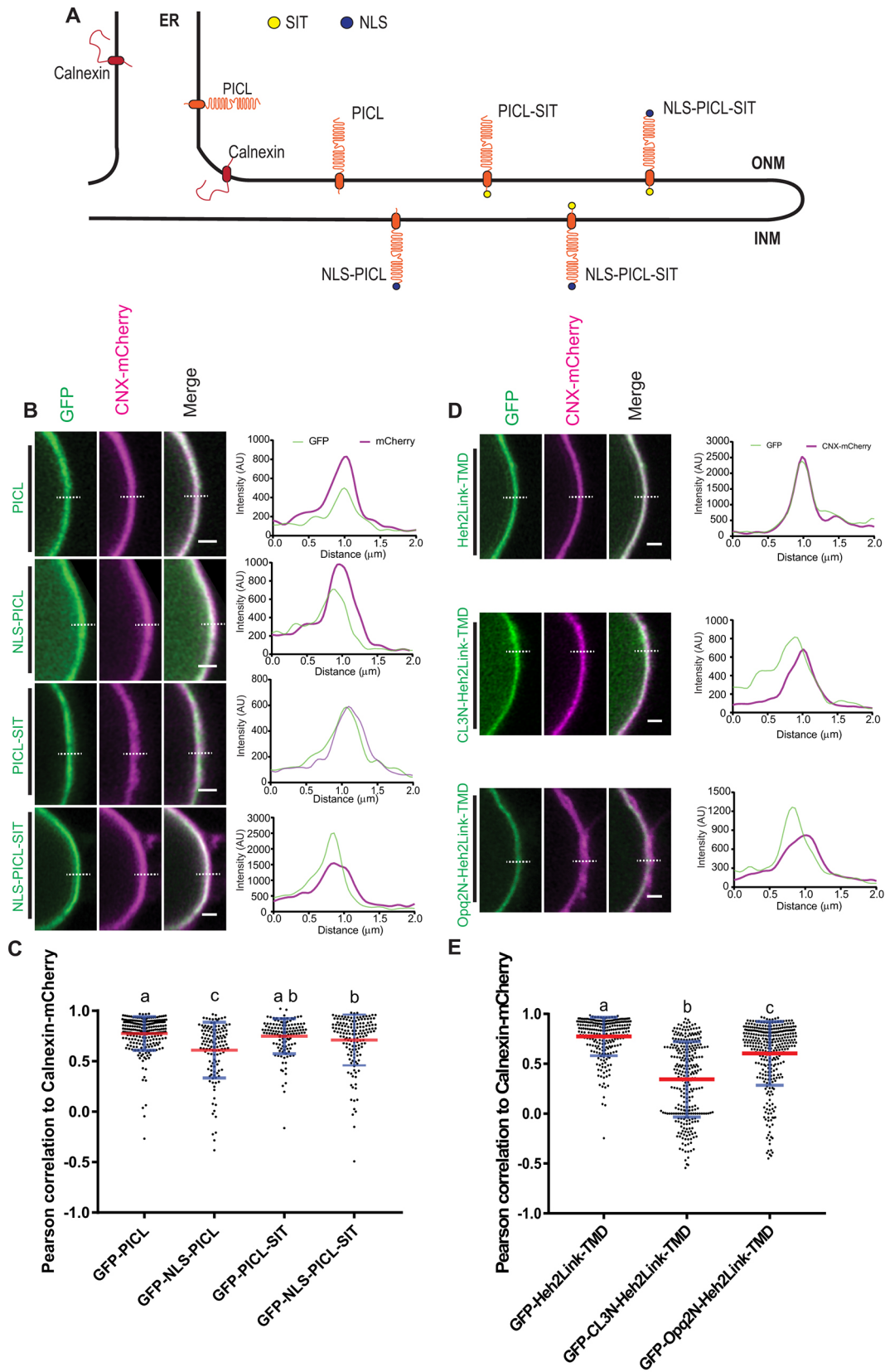


Fig. 8. See next page for legend.

located in the chloroplasts and GET3c in the mitochondria (Xing et al., 2017). The chimeric proteins developed here can now be used to query *Arabidopsis* with mutations in different GET pathway

components for involvement in INM targeting, a timely question regardless of which order of membrane insertion and nuclear pore trafficking has evolved in plants.

Fig. 8. NLS-fused ER membrane proteins and chimeric membrane proteins access the INM. Airyscan subdiffraction limited imaging demonstrates that the inclusion of an NLS with PICL, or with Heh2Link proteins allow proteins to access the INM. (A) Figure showing the localization relative to the ER, ONM and INM of the PICL variants used for imaging. (B) Representative images and corresponding line profiles of GFP-PICL, GFP-NLS-PICL, GFP-PICL-SIT and GFP-NLS-PICL-SIT colocalized with calnexin-mCherry. (C) Pearson's colocalization correlation of PICL variants and calnexin-mCherry. (D) Representative images and corresponding line profiles of chimeric membrane proteins Heh2Linker-TMD (Heh2Link-TMD), and CL3 NLS- and Opq2 NLS-fused varieties. In B and D, white dotted lines indicate the area at which line profiles were taken. Scale bars: 1 μ m. (E) Pearson's colocalization and correlation of Heh2Linker (Heh2Link) and corresponding NLS fusions with calnexin-mCherry. In C and E, a one-way ANOVA statistical test was performed, and groups that are statistically different from each other are denoted by different lowercase letters [$P < 0.05$ (a to b); $P < 0.0001$ (a to c); $P < 0.001$ (b to c); see Table S2]. In the plots, blue lines indicate error bars showing standard deviation, and red lines show the mean value. $n \geq 20$ nuclei across three experimental repeats with a minimum of 120 areas used for colocalization analysis.

The rules for targeting proteins to the INM laid out here can now be utilized to add new functionalities to the plant nuclear periphery. Plants lack a clearly defined nuclear lamina, and lack homologs of the proteins that tether chromatin to the nuclear periphery in other systems, LEM domain proteins and LBR. The chimeric membrane proteins detailed here could be used as a tool to potentially tether loci to the nuclear periphery or to artificially sequester proteins, such as chromatin remodeling factors, at the INM. This could provide an experimentally feasible approach towards understanding the role that the nuclear periphery can play in plant gene regulation.

MATERIALS AND METHODS

Plant materials

Plants were germinated on 0.5 \times Murashige and Skoog (Caisson Laboratories) plates containing 1% sucrose, and grown for 5 days post-germination prior to transferring to soil. *Nicotiana benthamiana* plants (gift from David E. Somers, Ohio State University, Columbus, OH) were grown at 28°C in soil under 16 h light, 8 h dark conditions.

Constructs and cloning

PICL cDNA (At1G05320) in the pENTR/D-Topo binary vector was described previously (Venkatakrishnan et al., 2013). NLS-PICL was generated by PCR amplification of the PICL open reading frame with two overlapping 5' primers containing the SV40 T-Antigen NLS (PICLNLSIF and PICLNLSIIF, all primer sequences are listed in Table S3) and 3' reverse primer (PICLR). PICL-SIT was generated by amplifying the PICL open reading frame with the 5' forward primer PICLF and the 3' reverse primer containing the SUN-interacting tail (SIT) from the Arabidopsis KASH protein WIP1 (PICLSITR) (Zhou et al., 2012). NLS-PICL-SIT was generated by amplifying the PICL open reading frame using overlapping forward primers that contain the SV40 T-Antigen NLS (PICLNLSIF and PICLNLSIIF) and reverse primers that contain SIT (PICLSITR). The PCR products generated above were introduced into the binary entry vector pENTR/D-Topo using the pENTR/D-Topo kit (Invitrogen, #45-0218). Constructs were introduced into the N-terminal GFP fusion plant overexpression vector pK7WGF2 (Karimi et al., 2002) via LR reaction (Invitrogen, #11791-020).

The *Saccharomyces cerevisiae* Heh2 open reading frame was amplified using primers designed for use in the GATEWAY system, based on primer sequences detailed in Meinema et al. (2011). Primers ScHeh2F and ScHeh2R were used to amplify the Heh2 open reading frame, which was inserted into the binary entry vector pENTR/D-Topo. The Heh2 fragments Heh2NLS-L-TM and Heh2L-TM were generated according to amino acid positions previously specified (Meinema et al., 2011). Heh2NLS-L-TM was amplified using the primers Heh2NLSF and Heh2TMR, and using ScHeh2 in pENTR/D-Topo as template. Heh2L-TM was amplified using the primers

Heh2LinkF and Heh2TMR. Heh2NLS-L-TM and Heh2L-TM were introduced into pENTR/D-Topo as described above. ScHeh2, Heh2NLS-L-TM, and Heh2L-TM were introduced into pK7WGF2 via an LR reaction.

For the purpose of generating chimeric membrane proteins, a GATEWAY destination vector was designed to allow for simultaneous N-terminal GFP tagging and C-terminal TMD fusion. A modified pK7WGF2 destination vector was generated that contained a *SpeI* site 5' of the GFP tag, and a *PmlI* site between the GATEWAY cassette and terminator (pK7WGF2 Mod, plasmid map available upon request). The *SpeI* and *PmlI* sites were introduced into pK7WGF2 via PCR using primers pKSpeIF and pKXba1R. The transmembrane domain (TMD) from *Arabidopsis thaliana* WIP1 (amino acids 452–482) was PCR amplified from the previously published WIP1 sequence in pENTR/D-topo clone (Zhou et al., 2012), using the primers WIP1TMDInFusF and WIP1TMDInFusR. The amplified WIP1 TMD was integrated into *PmlI*-digested pK7WGF2 Mod via InFusion reaction (Clontech Item #638912). The resulting vector, pK7TMW0WGF2, was sequenced-confirmed to be in-frame and error-free.

Heh2Linker-TMD was generated by PCR amplification of the domain between the Heh2NLS and TMD (amino acids 138–283) (Meinema et al., 2011), using primers Heh2LinkTopoF and LinkITopoR. The resulting fragment, Heh2Linker Δ Stop, was inserted into pENTR/D-Topo, then recombined into the GFP- and TMD-fusion vector pK7TMW0WGF2, resulting in GFP-Heh2linker-TMD. NLS-fused varieties of Heh2Linker Δ Stop were generated via PCR with a 5' NLS-fused primer and the 3' reverse primer LinkITopoR (see Table S3 for a complete list of primers). The resulting NLS-Heh2Linker Δ Stop fragments were inserted into pENTR/D-Topo via a Topo reaction, and subsequently recombined into pK7TMW0WGF2 to generate NLS-fused chimeric membrane proteins.

WIP1Coiled-Coil Δ Stop was amplified from the WIP1 coding sequence in pENTR/D-Topo previously described (Zhou et al., 2012), using the primers CCTopoF and CCTopoR (see Table S3 for sequences). Monopartite NLS-fused varieties of WIP1Coiled-Coil Δ Stop were generated via PCR with a 5' NLS-fused WIP1Coiled-Coil forward primer and CCTopoR. The resulting coiled-coil varieties were inserted into pENTR/D-Topo, then recombined into the GFP- and TMD- fusion vector pK7TMW0WGF2 via LR Reaction.

To generate short linker fragments, Heh2Linker Δ Stop in pENTR/D-Topo was used as a template. Fragments comprising 10 amino acids, 50 amino acid and 100 amino acids of the Heh2Linker region were generated through amplification with an NLS-fused forward primer annealing to the transcriptional start site, and a 3' primer annealing downstream to generate either a 30 bp, 150 bp, or 300 bp Heh2Linker fragment (see Table S3 for primer sequences). Additionally, the reverse primers introduced a *HindIII* restriction site, to be used for introducing additional features (see Table S4 for full list of plasmids). The NLS-fused Heh2Linker short fragments were introduced into pENTR/D-Topo, and subsequently recombined into pK7TMW0WGF2 via an LR reaction.

GATEWAY vectors were engineered to introduce an NLS 5' of the GFP coding sequence, in order to test whether NLSs were functional in soluble protein transport. Nine total NLSs were selected for use in this study (see Table S1 for NLS sequences and origin). Each NLS was generated by annealing and extending primers containing the NLS sequence and a complementary sequence to the *SpeI* site and flanking sequence in the modified pK7WGF2 vector (see Table S3 for a complete list of primers). The resulting NLSs were inserted into the *SpeI*-cut modified pK7WGF2 vector via InFusion reaction. Nine total vectors were generated, with each vector resulting in 35SProm::NLS-GFP-GW. The vectors were sequenced, and named pK7WGF2XN2, where 'XN' refers to the NLS used (see Table S4 for a full list of vectors and plasmids). GUS was amplified by PCR with the primers GUSF and GUSR, and inserted into pENTR/D-Topo. GUS was inserted into each 35SProm::NLS-GUS-GW vector, as well as the modified pK7WGF2, to generate NLS-GFP-GUS for testing soluble protein import of NLS-bound GFP-GUS.

Heh2 short linker fragments previously described contained a *HindIII* restriction site at the 3' end of the fragment. A Heh2linker fragment was amplified to insert *HindIII* restriction sites on the 5' and 3' end to generate Heh2Linker-DualH3 (see Table S3 for primers and Table S4 for a list of plasmids). SV40NLS-fused short linker fragments in D-Topo were digested with *HindIII*, as was Heh2Linker-DualH3. The *HindIII*-digested

Heh2Linker-DualH3 was ligated into each digested SV40NLS-fused short linker to generate SV40NLS-Link200, SV40NLS-Link250 and SV40NLS-Link300 (T4 DNA ligase, NEB #M202S). The resulting NLS-fused long linker fragments were inserted into pK7TMW0WGF2, the N-terminal GFP- and C-terminal TMD- fusion plant overexpression vector.

Agrobacterium transformation

Agrobacterium tumefaciens strain ABI (gift from David E. Somers) was transformed with individual plasmids by triparental mating (Wise et al., 2006). *E. coli* containing plasmids of interest were mixed with *Agrobacterium* strain ABI and the *E. coli* helper strain containing the pRK2013 vector. The bacterial mixture was incubated overnight at 30°C on Lysogeny broth (LB) agar (1.5%) plates. Then, the bacteria were streaked onto LB (1.5%) plates containing appropriate antibiotics to select for transformed *Agrobacterium*. Transformed *Agrobacterium* colonies were confirmed via PCR amplification of the insert prior to use in subsequent experiments.

N. benthamiana transient transformation

Agrobacterium cultures containing plasmids expressing proteins of interest were co-infiltrated into *N. benthamiana* leaves as previously described (Sparkes et al., 2006). *Agrobacterium* cultures were centrifuged (2400 g for 15 min) and resuspended at an optical density at 600 nm (OD_{600})=1.0 in infiltration buffer containing 10 mM MgCl₂, 10 mM MES, pH 5.4, and 100 μM acetosyringone. The *Agrobacterium* suspension was pressure infiltrated into *N. benthamiana* leaves using a flat-tipped plastic syringe applied to the abaxial side of the leaf. Infiltration sites were primed prior to infiltration using a syringe needle. Histone 2B-mCherry (H2B-Cherry) was co-infiltrated as a nuclear marker (Newman-Griffis et al., 2019). Plants were grown for 3 days post-infiltration prior to imaging.

Confocal microscopy

N. benthamiana leaves 3 days post-infiltration were imaged using a Nikon Eclipse C90i confocal microscope with small or medium pinhole and gain setting between 5.0 and 7.5. The 488 nm laser was set to 10–30% laser power and the 561 nm laser was set to 5–30% laser power for all imaging experiments. Images were collected using the Nikon Plan Apo VC 60× H lens (1.4 NA). The transmitted light detector was turned on to collect transmitted signal simultaneously. Fluorescence intensity for subsequent analyses was measured in NIS-Elements software. Images were exported as PNG files and assembled into figures in Adobe Illustrator.

Nuclear envelope enrichment quantification

A nuclear localization index (NLI) was calculated as previously described (Zhou et al., 2012). In short, fluorescence intensity was measured across a line drawn through the nuclear envelope, as well as ER contact sites at the cell periphery. The two highest nuclear envelope fluorescence values were divided by the two highest ER values, resulting in the NLI. A minimum of 20 nuclei were used per membrane protein for NLI analysis.

Airyscan confocal microscopy

Airyscan subdiffraction limited microscopy was performed on a Zeiss LSM880 microscope. A 100×/1.46NA DIC M27 Elyra oil immersion lens was used. A dual emission filter was used combining 500–550 nm band pass and 565 nm long pass filters and a 615 nm short pass filter was used to block chlorophyll autofluorescence. GFP was excited with a 488 nm laser and mCherry with a 561 nm laser both set at 1% power. Bi-directional scanning and line sequential imaging was used. Averaging (4×) was performed, and a digital zoom (5×) with frame size of 404×404 pixels, which is optimum for Airyscan imaging, was used.

Airyscan quantification

Quantification of colocalization between labeled proteins (CFP, GFP or YFP) and an ONM/ER marker (mCherry) was performed by calculating the Pearson's colocalization coefficient in Zen Blue V2.3.69.1000. Colocalization analysis was performed on six areas for every nucleus imaged. Each area corresponded to a section of the nucleus in focus containing both labeled protein (CFP, GFP and YFP) and calnexin (RFP)

signal. A minimum of 20 nuclei in three experimental repeats were imaged and quantified, and exact number of nuclei for each experiment is listed in the figure legends. Graphs were compiled in Graphpad prism V7.04 and a one-way ANOVA with multiple comparisons test was performed.

Determining the ratio of INM to ONM fluorescence by means of Airyscan subdiffraction limited microscopy

In order to determine the ratio of INM and ONM signal that Airyscan subdiffraction imaging could resolve, the following was performed. Images were converted to 8-bit with minimum and maximum values scaled in FIJI (as is standard). Calnexin-mCherry images were then subtracted from those for WIP1 (GFP, ONM), SUN2 (CFP, INM) or CRWN1 (YFP, nuclear periphery) using the image calculator in FIJI. Identical line profiles for WIP1, SUN2 or CRWN1 and subtracted images were generated using the region of interest (ROI) manager in FIJI. The subtracted channel maximum intensity value was then divided by the maximum intensity value for CFP, GFP or YFP to give the ratio of the marker fluorescence to ONM fluorescence. These values were collated in excel and scatter plots drawn in Graphpad. A one-way ANOVA statistical test with multiple comparisons was performed.

FRAP

FRAP was performed on a Zeiss LSM880 confocal system with a 100×1.46 NA lens. GFP was excited with the 488 nm laser and emission collected at 500–550 nm. A 5× digital zoom was used. For bleaching, five prebleach frames were taken and then a centered ROI of 200×200 pixels was bleached for 50 iterations with the laser at 100% power; 235 post bleach frames were required with an acquisition of 0.13 s. A minimum number of 30 nuclei were imaged across three experimental repeats. The normalized intensity for each bleach curve was determined as previously described (Martiniere et al., 2012). Data were collated in Graphpad and one-phase association curves produced over 20 s. Plateau and half-time values were then determined and plotted as plots with each individual value and the mean±s.d. One-way ANOVA statistical tests were performed to compare the different conditions.

Acknowledgements

N.R.G. would like to thank Dr Xiao Zhou for ideas and guidance at the onset of this project, and Anna Newman-Griffis, Alecia Biel and the rest of the Meier laboratory for fruitful discussions. N.R.G. and I.M. wish to thank Dr Margaret Evans for accommodation and wonderful hospitality during imaging visits at Oxford Brookes University.

Competing interests

The authors declare no competing or financial interests.

Author contributions

Conceptualization: N.R.G., I.M.; Methodology: N.R.G., J.F.M., K.G.; Validation: N.R.G., J.F.M.; Formal analysis: N.R.G., J.F.M.; Investigation: N.R.G., J.F.M., I.M.; Resources: D.E.E., K.G., I.M.; Writing - original draft: N.R.G., J.F.M., I.M.; Writing - review & editing: D.E.E., I.M.; Supervision: D.E.E., K.G., I.M.; Project administration: I.M.; Funding acquisition: D.E.E., I.M.

Funding

Work in the Meier laboratory was supported by funding from the National Science Foundation (NSF-1440019 and NSF-1613501). J.F.M., D.E.E. and K.G. would like to thank Oxford Brookes University for funding.

Supplementary information

Supplementary information available online at <http://jcs.biologists.org/lookup/doi/10.1242/jcs.226134.supplemental>

References

- Barton, L. J., Soshnev, A. A. and Geyer, P. K. (2015). Networking in the nucleus: a spotlight on LEM-domain proteins. *Curr. Opin. Cell Biol.* **34**, 1–8.
- Boni, A., Politi, A. Z., Strnad, P., Xiang, W., Hossain, M. J. and Ellenberg, J. (2015). Live imaging and modeling of inner nuclear membrane targeting reveals its molecular requirements in mammalian cells. *J. Cell Biol.* **209**, 705–720.
- Capoen, W., Sun, J., Wysham, D., Otegui, M. S., Venkateshwaran, M., Hirsch, S., Miwa, H., Downie, J. A., Morris, R. J., Ané, J.-M. et al. (2011). Nuclear membranes control symbiotic calcium signaling of legumes. *Proc. Natl. Acad. Sci. USA* **108**, 14348–14353.

- Dang, C. V. and Lee, W. M. (1988). Identification of the human c-myc protein nuclear translocation signal. *Mol. Cell. Biol.* **8**, 4048-4054.
- de Las Heras, J. I., Meinke, P., Batrakou, D. G., Srsen, V., Zuleger, N., Kerr, A. R. and Schirmer, E. C. (2013). Tissue specificity in the nuclear envelope supports its functional complexity. *Nucleus* **4**, 1-18.
- Dittmer, T. A., Stacey, N. J., Sugimoto-Shirasu, K. and Richards, E. J. (2007). LITTLE NUCLEI genes affecting nuclear morphology in *Arabidopsis thaliana*. *Plant Cell* **19**, 2793-2803.
- Goto, C., Tamura, K., Fukao, Y., Shimada, T. and Hara-Nishimura, I. (2014). The novel nuclear envelope protein KAKU4 modulates nuclear morphology in *Arabidopsis*. *Plant Cell* **26**, 2143-2155.
- Graumann, K., Irons, S. L., Runions, J. and Evans, D. E. (2007). Retention and mobility of the mammalian lamin B receptor in the Plant Nuclear Envelope. *Biol. Cell* **99**, 553-562.
- Graumann, K., Runions, J. and Evans, D. E. (2010). Characterization of SUN-domain proteins at the higher plant nuclear envelope. *Plant J.* **61**, 134-144.
- Graumann, K., Vanrobays, E., Tutois, S., Probst, A. V., Evans, D. E. and Tatout, C. (2014). Characterization of two distinct subfamilies of SUN-domain proteins in *Arabidopsis* and their interactions with the novel KASH-domain protein ATTIK. *J. Exp. Bot.* **65**, 6499-6512.
- Grossman, E., Medalia, O. and Zwerger, M. (2012). Functional architecture of the nuclear pore complex. *Annu. Rev. Biophys.* **41**, 557-584.
- Huff, J. (2015). The Airyscan detector from ZEISS: confocal imaging with improved signal-to-noise ratio and super-resolution. *Nat. Methods* **12**, 1205.
- Irons, S. L., Evans, D. E. and Brandizzi, F. (2003). The first 238 amino acids of the human lamin B receptor are targeted to the nuclear envelope in plants. *J. Exp. Bot.* **54**, 943-950.
- Janin, A., Bauer, D., Ratti, F., Millat, G. and Méjat, A. (2017). Nuclear envelopathies: a complex LINC between nuclear envelope and pathology. *Orphanet J. Rare Dis.* **12**, 1-16.
- Jefferson, R. A., Kavanagh, T. A. and Bevan, M. W. (1987). GUS fusions: beta-glucuronidase as a sensitive and versatile gene fusion marker in higher plants. *EMBO J.* **6**, 3901-3907.
- Kalderon, D., Roberts, B. L., Richardson, W. D. and Smith, A. E. (1984). A short amino acid sequence able to specify nuclear location. *Cell* **39**, 499-509.
- Karimi, M., Inzé, D. and Depicker, A. (2002). GATEWAY™ vectors for Agrobacterium-mediated plant transformation. *Trends Plant Sci.* **7**, 193-195.
- Katta, S. S., Smoyer, C. J. and Jaspersen, S. L. (2014). Destination: inner nuclear membrane. *Trends Cell Biol.* **24**, 221-229.
- Kim, S. J., Fernandez-Martinez, J., Nudelman, I., Shi, Y., Zhang, W., Raveh, B., Herricks, T., Slaughter, B. D., Hogan, J. A., Upla, P. et al. (2018). Integrative structure and functional anatomy of a nuclear pore complex. *Nature* **555**, 475-482.
- King, M. C., Lusk, C. P. and Blobel, G. (2006). Karyopherin-mediated import of integral inner nuclear membrane proteins. *Nature* **442**, 1003-1007.
- Korfali, N., Wilkie, G. S., Swanson, S. K., Srsen, V., de Las Heras, J., Batrakou, D. G., Malik, P., Zuleger, N., Kerr, A. R. W., Florens, L. et al. (2012). The nuclear envelope proteome differs notably between tissues. *Nucleus* **3**, 552-564.
- Korobchevskaya, K., Lagerholm, B., Colin-York, H. and Fritzsche, M. (2017). Exploring the potential of Airyscan microscopy for live cell imaging. *Photonics* **4**, 41.
- Kosugi, S., Hasebe, M., Matsumura, N., Takashima, H., Miyamoto-Sato, E., Tomita, M. and Yanagawa, H. (2009). Six classes of nuclear localization signals specific to different binding grooves of importin alpha. *J. Biol. Chem.* **284**, 478-485.
- Kralt, A., Jagalur, N. B., van den Boom, V., Lokareddy, R. K., Steen, A., Cingolani, G., Fornerod, M. and Veenhoff, L. M. (2015). Conservation of inner nuclear membrane targeting sequences in mammalian Pom121 and yeast Heh2 membrane proteins. *Mol. Biol. Cell* **26**, 3301-3312.
- Laba, J., Steen, A., Popken, P., Chernova, A., Poolman, B. and Veenhoff, L. (2015). Active nuclear import of membrane proteins revisited. *Cells* **4**, 653-673.
- Lange, A., Mills, R. E., Lange, C. J., Stewart, M., Devine, S. E. and Corbett, A. H. (2007). Classical nuclear localization signals: definition, function, and interaction with importin α . *J. Biol. Chem.* **282**, 5101-5105.
- Liu, D., Wu, X., Summers, M. D., Lee, A., Ryan, K. J. and Braunagel, S. C. (2010). Truncated isoforms of Kap60 facilitate trafficking of Heh2 to the nuclear envelope. *Traffic* **11**, 1506-1518.
- Liu, D. Y. T., Smith, P. M. C., Barton, D. A., Day, D. A. and Overall, R. L. (2017). Characterisation of *Arabidopsis* calnexin 1 and calnexin 2 in the endoplasmic reticulum and at plasmodesmata. *Protoplasma* **254**, 125-136.
- Lokareddy, R. K., Hapsari, R. A., van Rheenen, M., Pumroy, R. A., Bhardwaj, A., Steen, A., Veenhoff, L. M. and Cingolani, G. (2015). Distinctive properties of the nuclear localization signals of inner nuclear membrane proteins Heh1 and Heh2. *Structure* **23**, 1305-1316.
- Lyman, S. K., Guan, T., Bednenko, J., Wodrich, H. and Gerace, L. (2002). Influence of cargo size on Ran and energy requirements for nuclear protein import. *J. Cell Biol.* **159**, 55-67.
- Martiniere, A., Lavagi, I., Nageswaran, G., Rolfe, D. J., Maneta-Peyret, L., Luu, D.-T., Botchway, S. W., Webb, S. E. D., Mongrand, S., Maurel, C. et al. (2012). Cell wall constrains lateral diffusion of plant plasma-membrane proteins. *Proc. Natl. Acad. Sci. USA* **109**, 12805-12810.
- Meier, I., Richards, E. J. and Evans, D. E. (2017). Cell biology of the plant nucleus. *Annu. Rev. Plant Biol.* **68**, 139-172.
- Meinema, A. C., Laba, J. K., Hapsari, R. A., Otten, R., Mulder, F. A. A., Kralt, A., van den Bogaart, G., Lusk, C. P., Poolman, B. and Veenhoff, L. M. (2011). Long unfolded linkers facilitate membrane protein import through the nuclear pore complex. *Science* **333**, 90-93.
- Meinema, A. C., Poolman, B. and Veenhoff, L. M. (2013). Quantitative analysis of membrane protein transport across the nuclear pore complex. *Traffic* **14**, 487-501.
- Merkle, T. (2011). Nucleo-cytoplasmic transport of proteins and RNA in plants. *Plant Cell Rep.* **30**, 153-176.
- Mitchell, J. M., Mansfield, J., Capitanio, J., Kutay, U. and Wozniak, R. W. (2010). Pom121 links two essential subcomplexes of the nuclear pore complex core to the membrane. *J. Cell Biol.* **191**, 505-521.
- Mosalaganti, S., Kosinski, J., Albert, S., Schaffer, M., Strenkert, D., Salomé, P. A., Merchant, S. S., Plietzko, J. M., Baumeister, W., Engel, B. D. et al. (2018). In situ architecture of the algal nuclear pore complex. *Nat. Commun.* **9**, 1-8.
- Mudumbi, K. C., Schirmer, E. C., Yang, W., Arib, G., Akhtar, A., Burns, L. T., Wente, S. R., de las Heras, J. I., Gruenbaum, Y., Margalit, A. et al. (2016). Single-point single-molecule FRAP distinguishes inner and outer nuclear membrane protein distribution. *Nat. Commun.* **7**, 12562.
- Newman-Griffis, A. H., Del Cerro, P., Charpentier, M. and Meier, I. (2019). Medicago LINC complexes function in nuclear morphology, nuclear movement, and root nodule symbiosis. *Plant Physiol.* **179**, 491-506.
- Nikolakaki, E., Mylonis, I. and Giannakouros, T. (2017). Lamin B receptor: interplay between structure, function and localization. *Cells* **6**, 28.
- Patel, S. S., Belmont, B. J., Sante, J. M. and Rexach, M. F. (2007). Natively unfolded nucleoporins gate protein diffusion across the nuclear pore complex. *Cell* **129**, 83-96.
- Popken, P., Ghavami, A., Onck, P. R., Poolman, B. and Veenhoff, L. M. (2015). Size-dependent leak of soluble and membrane proteins through the yeast nuclear pore complex. *Mol. Biol. Cell* **26**, 1386-1394.
- Poulet, A., Probst, A. V., Graumann, K., Tatout, C. and Evans, D. (2017). Exploring the evolution of the proteins of the plant nuclear envelope. *Nucleus* **8**, 46-59.
- Powell, L. and Burke, B. (1990). Internuclear exchange of an inner nuclear membrane protein (p55) in heterokaryons: in vivo evidence for the interaction of p55 with the nuclear lamina. *J. Cell Biol.* **111**, 2225-2234.
- Robbins, J., Dilworth, S. M., Laskey, R. A. and Dingwall, C. (1991). Two interdependent basic domains in nucleoplasmin nuclear targeting sequence: identification of a class of bipartite nuclear targeting sequence. *Cell* **64**, 615-623.
- Rothballer, A., Schwartz, T. U. and Kutay, U. (2013). LINCing complex functions at the nuclear envelope. *Nucleus* **4**, 29-36.
- Saksena, S., Summers, M. D., Burks, J. K., Johnson, A. E. and Braunagel, S. C. (2006). Importin-alpha-16 is a translocon-associated protein involved in sorting membrane proteins to the nuclear envelope. *Nat. Struct. Mol. Biol.* **13**, 500-508.
- Shao, S. and Hegde, R. S. (2011). Membrane Protein Insertion at the Endoplasmic Reticulum. *Annu. Rev. Cell Dev. Biol.* **27**, 25-56.
- Smith, S. and Blobel, G. (1993). The first membrane spanning region of the lamin B receptor is sufficient for sorting to the inner nuclear membrane. *J. Cell Biol.* **120**, 631-637.
- Smoyer, C. J., Katta, S. S., Gardner, J. M., Stoltz, L., McCroskey, S., Bradford, W. D., McClain, M., Smith, S. E., Slaughter, B. D., Unruh, J. R. et al. (2016). Analysis of membrane proteins localizing to the inner nuclear envelope in living cells. *J. Cell Biol.* **215**, 575-590.
- Soniati, M. and Chook, Y. M. (2015). Nuclear localization signals for four distinct karyopherin- β nuclear import systems. *Biochem. J.* **468**, 353-362.
- Soullam, B. and Worman, H. J. (1993). The amino-terminal domain of the lamin B receptor is a nuclear envelope targeting signal. *J. Cell Biol.* **120**, 1093-1100.
- Sparkes, I. A., Runions, J., Kearns, A. and Hawes, C. (2006). Rapid, transient expression of fluorescent fusion proteins in tobacco plants and generation of stably transformed plants. *Nat. Protoc.* **1**, 2019-2025.
- Starr, D. A. and Fridolfsson, H. N. (2010). Interactions between nuclei and the cytoskeleton are mediated by SUN-KASH nuclear-envelope bridges. *Annu. Rev. Cell Dev. Biol.* **26**, 421-444.
- Tamura, K. and Hara-Nishimura, I. (2012). The molecular architecture of the plant nuclear pore complex. *J. Exp. Bot.* **63**, 695-709.
- Tamura, K. and Hara-Nishimura, I. (2014). Functional insights of nucleocytoplasmic transport in plants. *Front. Plant Sci.* **5**, 118.
- Tamura, K., Fukao, Y., Iwamoto, M., Haraguchi, T. and Hara-Nishimura, I. (2010). Identification and characterization of nuclear pore complex components in *Arabidopsis thaliana*. *Plant Cell* **22**, 4084-4097.
- Tapley, E. C., Ly, N. and Starr, D. A. (2011). Multiple mechanisms actively target the SUN protein UNC-84 to the inner nuclear membrane. *Mol. Biol. Cell* **22**, 1739-1752.
- Turgay, Y., Ungricht, R., Rothballer, A., Kiss, A., Csucs, G., Horvath, P. and Kutay, U. (2010). A classical NLS and the SUN domain contribute to the targeting of SUN2 to the inner nuclear membrane. *EMBO J.* **29**, 2262-2275.
- Ungricht, R., Klann, M., Horvath, P. and Kutay, U. (2015). Diffusion and retention are major determinants of protein targeting to the inner nuclear membrane. *J. Cell Biol.* **209**, 687-704.

- Varagona, M. J., Schmidt, R. J. and Raikhel, N. V.** (1992). Nuclear localization signal(s) required for nuclear targeting of the maize regulatory protein Opaque-2. *Plant Cell* **4**, 1213-1227.
- Venkatakrishnan, S., Mackey, D. and Meier, I.** (2013). Functional investigation of the plant-specific long coiled-coil proteins PAMP-INDUCED COILED-COIL (PICC) and PICC-LIKE (PICL) in *Arabidopsis thaliana*. *PLoS ONE* **8**, e57283.
- Wang, R. and Brattain, M. G.** (2007). The maximal size of protein to diffuse through the nuclear pore is larger than 60 kDa. *FEBS Lett.* **581**, 3164-3170.
- Wang, H., Dittmer, T. A. and Richards, E. J.** (2013). *Arabidopsis* CROWDED NUCLEI (CRWN) proteins are required for nuclear size control and heterochromatin organization. *BMC Plant Biol.* **13**, 200.
- Wise, A. A., Liu, Z. and Binns, A. N.** (2006). Three methods for the introduction of foreign DNA in agrobacterium. *Methods Mol. Biol.*, **343**, 43-54.
- Xing, S., Mehlhorn, D. G., Wallmeroth, N., Asseck, L. Y., Kar, R., Voss, A., Denninger, P., Schmidt, V. A. F., Schwarzländer, M., Stierhof, Y.-D. et al.** (2017). Loss of GET pathway orthologs in *Arabidopsis thaliana* causes root hair growth defects and affects SNARE abundance. *Proc. Natl. Acad. Sci. USA* **114**, E1544-E1553.
- Xu, X. M., Meulia, T. and Meier, I.** (2007). Anchorage of plant RanGAP to the nuclear envelope involves novel nuclear-pore-associated proteins. *Curr. Biol.* **17**, 1157-1163.
- Zhou, X., Graumann, K., Evans, D. E. and Meier, I.** (2012). Novel plant SUN-KASH bridges are involved in RanGAP anchoring and nuclear shape determination. *J. Cell Biol.* **196**, 203-211.
- Zhou, X., Graumann, K., Wirthmueller, L., Jones, J. D. G. and Meier, I.** (2014). Identification of unique SUN-interacting nuclear envelope proteins with diverse functions in plants. *J. Cell Biol.* **205**, 677-692.
- Zuleger, N., Kelly, D. A., Richardson, A. C., Kerr, A. R. W., Goldberg, M. W., Goryachev, A. B. and Schirmer, E. C.** (2011). System analysis shows distinct mechanisms and common principles of nuclear envelope protein dynamics. *J. Cell Biol.* **193**, 109-123.

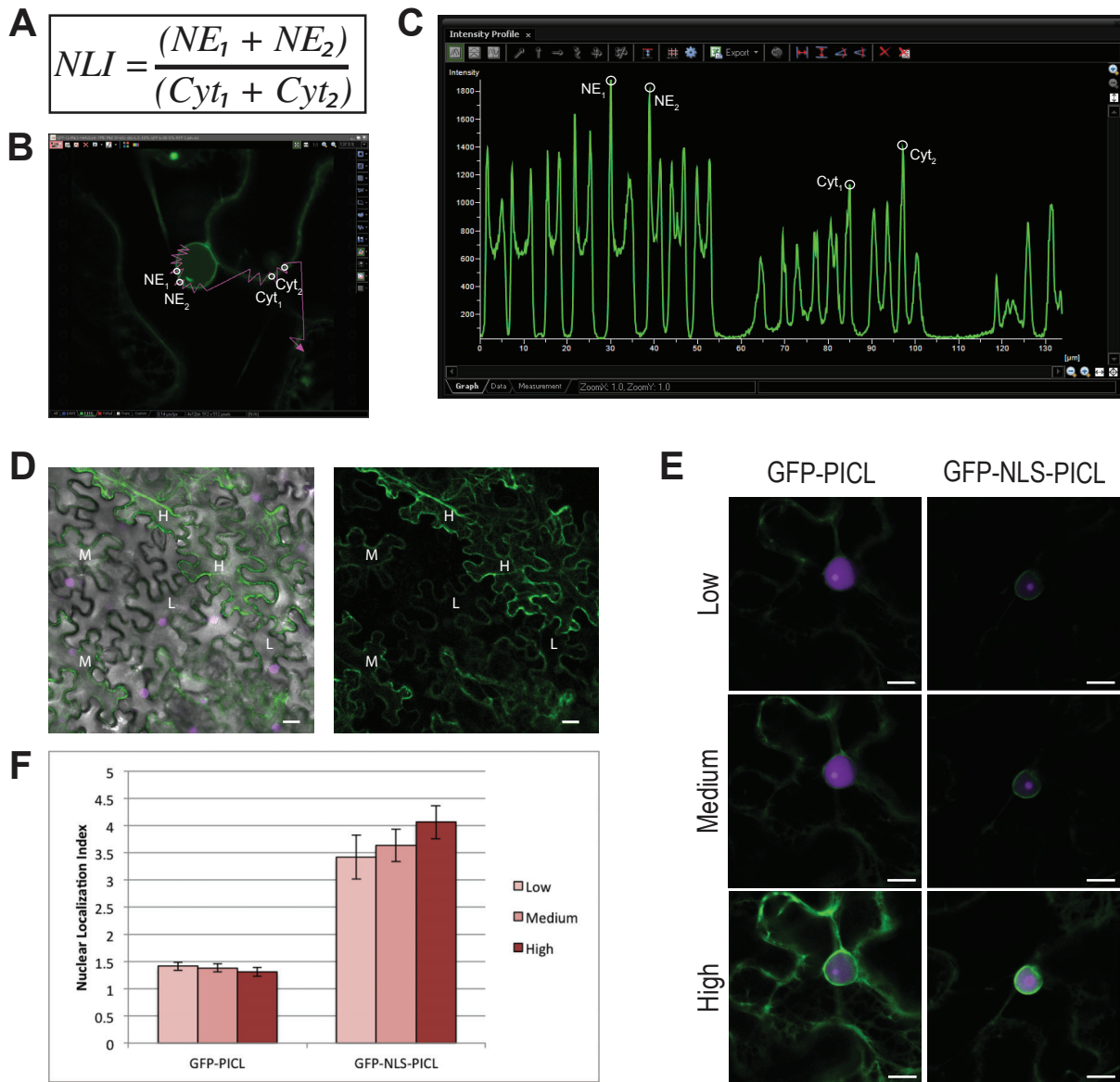


Figure S1. Illustration of data quantification protocol and definition of nuclear localization index as used in this study. **A.** The nuclear localization index (NLI) is calculated by taking the two highest NE fluorescence values and dividing by the two highest cytoplasmic signals, to give a measure of relative signal enrichment at the NE. **B.** Fluorescence intensity is measured along lines drawn through the nuclear envelope and ER contact sites at the cell periphery in Nikon NIS-Elements software. **C.** An example fluorescence intensity chart is shown. Maximal nuclear envelope (NE) and cytoplasmic (cyt) signal peaks are labeled. **D.** 20x magnification images of transiently transformed *N. benthamiana* leaf epidermal cells. High, medium, and low expressing cells are denoted by H, M, or L, respectively. A DIC/GFP merge is on the left, and GFP-only is on the right. Scale bars = 10 μ m. **E.** Medium expression cells for GFP-PICL or GFP-NLS-PICL, imaged under low, medium or high imaging conditions. High = 7.35 gain, 20% 488nm laser power, S pinhole. Medium = 7.35 gain, 30% 488nm laser power, S pinhole. Low = 7.35 gain, 20% 488nm Laser power, M pinhole. Scale bars = 10 μ m. **F.** Nuclear localization index of low, medium and high expressing cells of either GFP-PICL or GFP-NLS-PICL. N=12-26 nuclei per imaging condition.

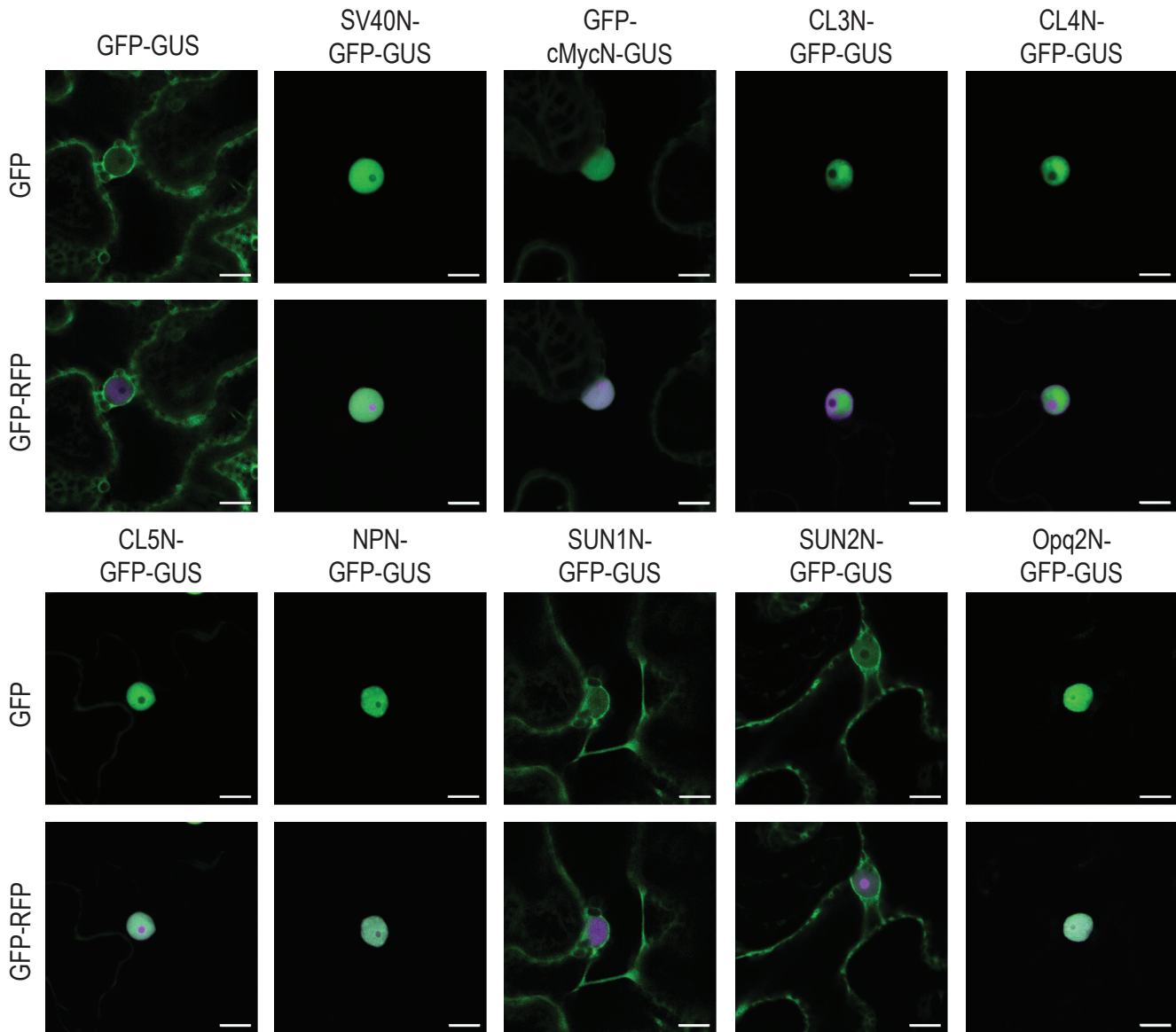


Figure S2. Nuclear localization signals are functional in soluble protein import.

Nuclear localization signals were fused to GFP-GUS to test the ability of NLSs to target a soluble protein to the nucleus. NLS-GFP-GUS proteins were transiently co-expressed with H2B-mCherry to mark the nucleus. Representative images are shown. Scale bars= 10 μ m.

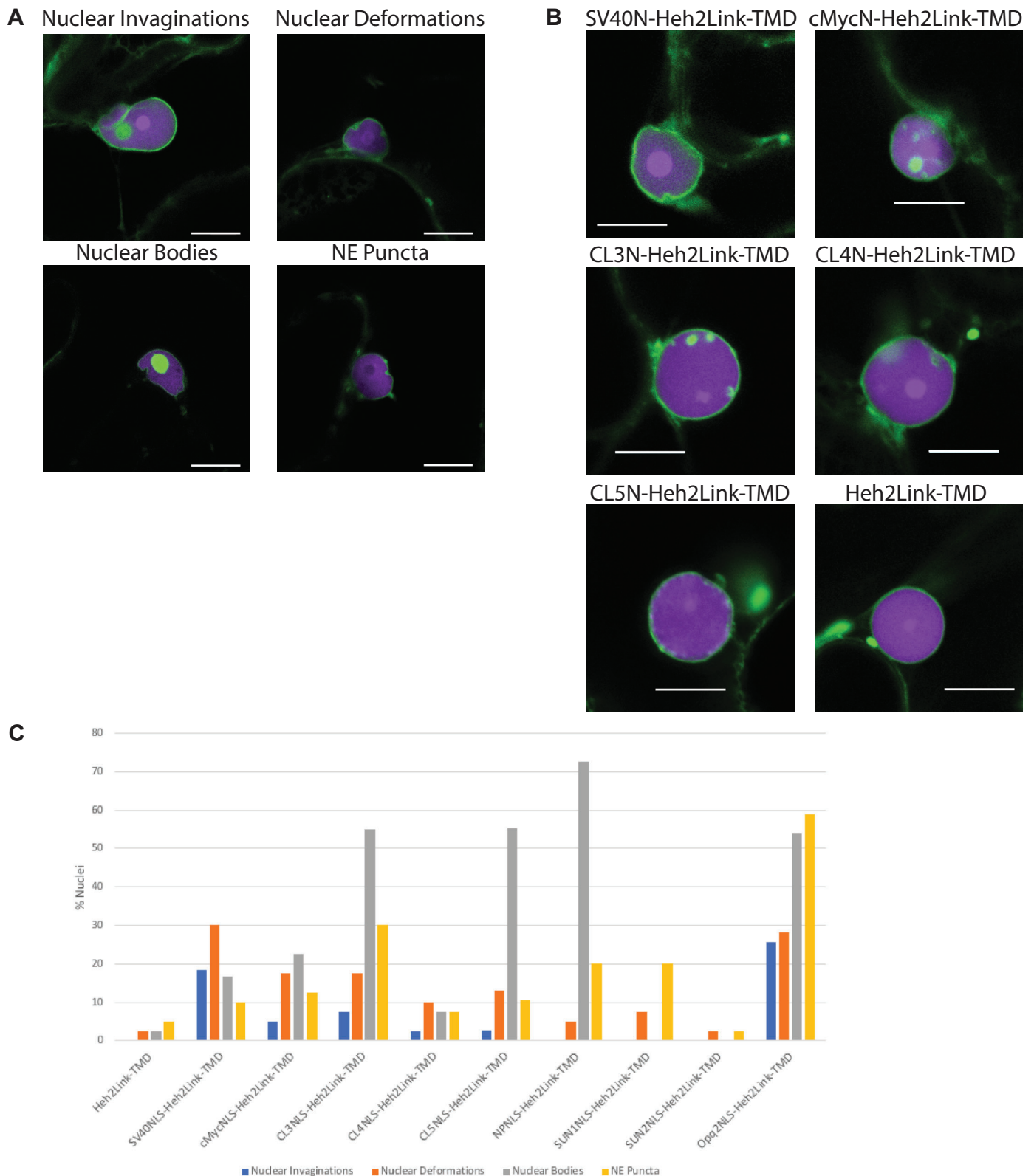


Figure S3. Overexpression of NLS-fused chimeric membrane proteins induces nuclear abnormalities. **A.** Example images of different nuclear abnormalities in *N. benthamiana* leaf epidermal cells overexpressing chimeric membrane proteins. Scale bars = 10µm. **B.** Representative images of monopartite NLS-fused chimeric membrane proteins in *N. benthamiana*. Scale bars = 10µm. **C.** Nuclear abnormalities were scored for a population of 40 nuclei for Heh2Linker-TMD and NLS-Heh2Linker-TMD chimeric membrane proteins. Abnormalities are represented as a percentage of the population.

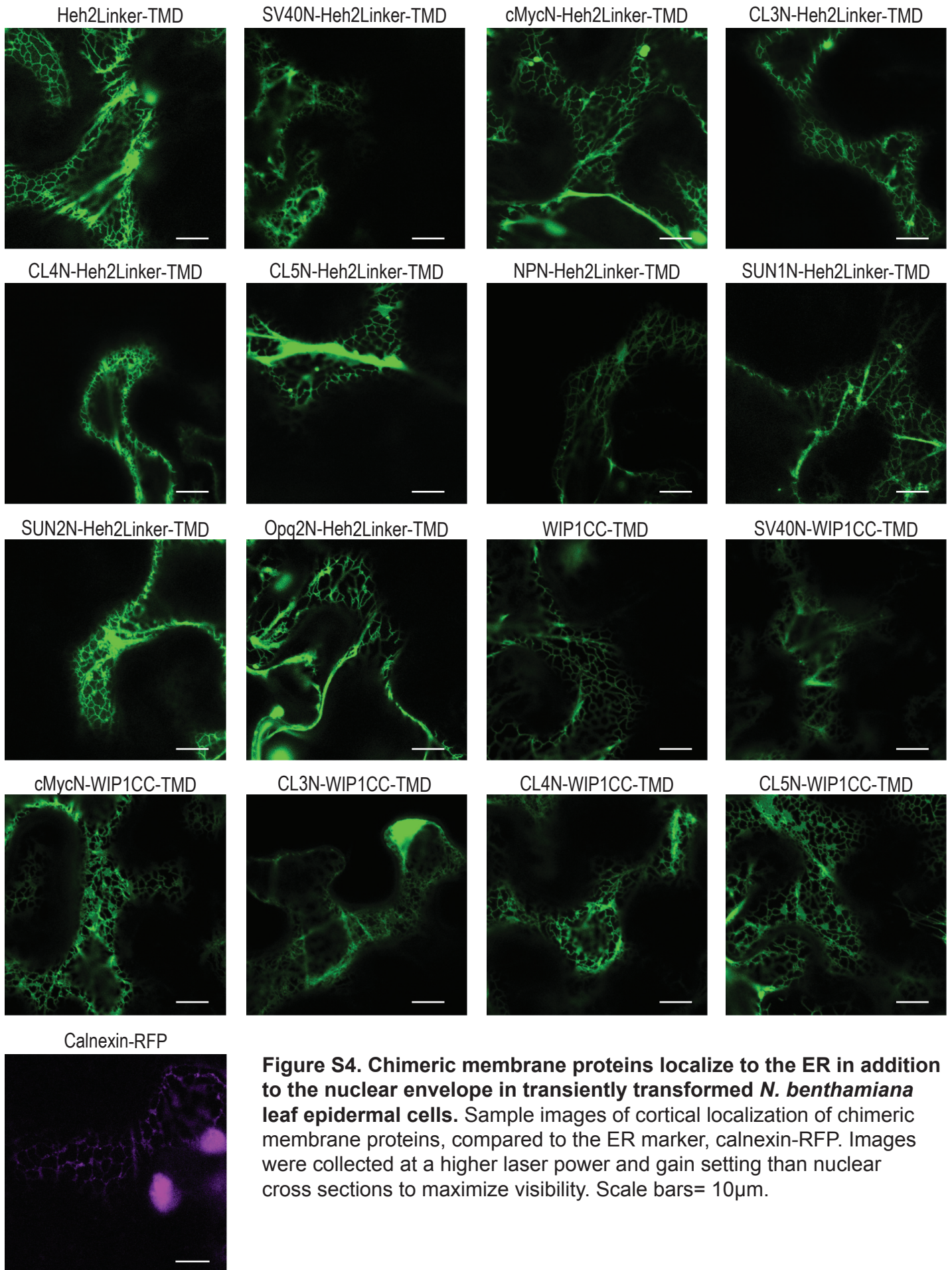


Figure S4. Chimeric membrane proteins localize to the ER in addition to the nuclear envelope in transiently transformed *N. benthamiana* leaf epidermal cells. Sample images of cortical localization of chimeric membrane proteins, compared to the ER marker, calnexin-RFP. Images were collected at a higher laser power and gain setting than nuclear cross sections to maximize visibility. Scale bars= 10µm.

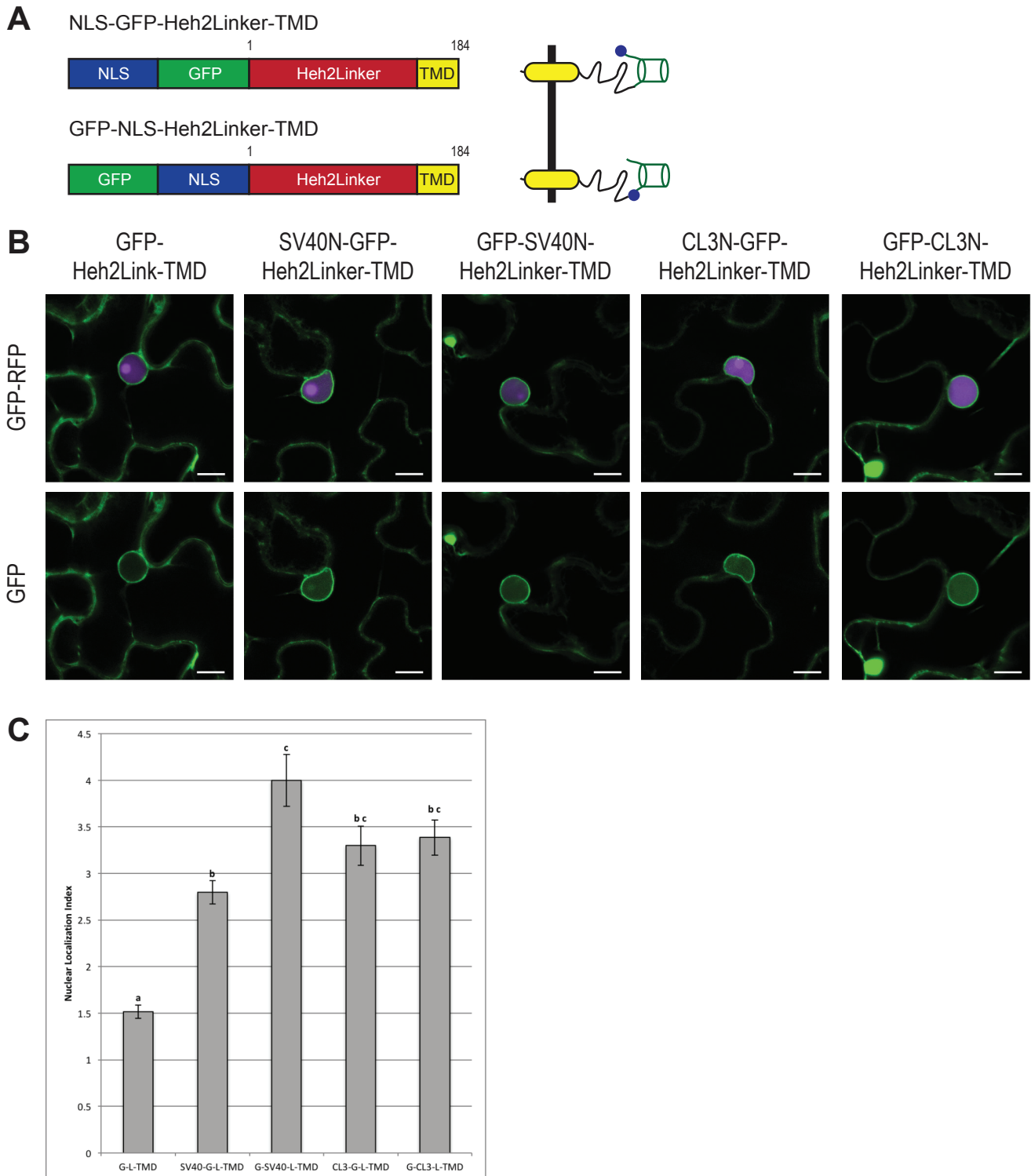


Figure S5. N-terminal vs internal position of the NLS does not significantly impact NE enrichment. **A.** GFP-NLS-Heh2Linker-TMD and NLS-GFP-Heh2Linker-TMD are diagrammed. GFP-NLS-Heh2Linker-TMD was generated as detailed in Figure 3, and NLS-GFP-Heh2Linker-TMD was generated as described in methods. NLS and GFP not drawn to scale. **B.** GFP fusions of chimeric membrane proteins were transiently expressed in *N. benthamina* leaf epidermal cells, along with the nuclear marker H2B-mCherry. Scale bars= 10µm. **C.** NLIs were calculated for all chimeric membrane proteins. Statistical significance was calculated using Student's T-test, and statistical groups are denoted by letters. $p < 0.001$. Error bars denote standard error. N=40 cells.

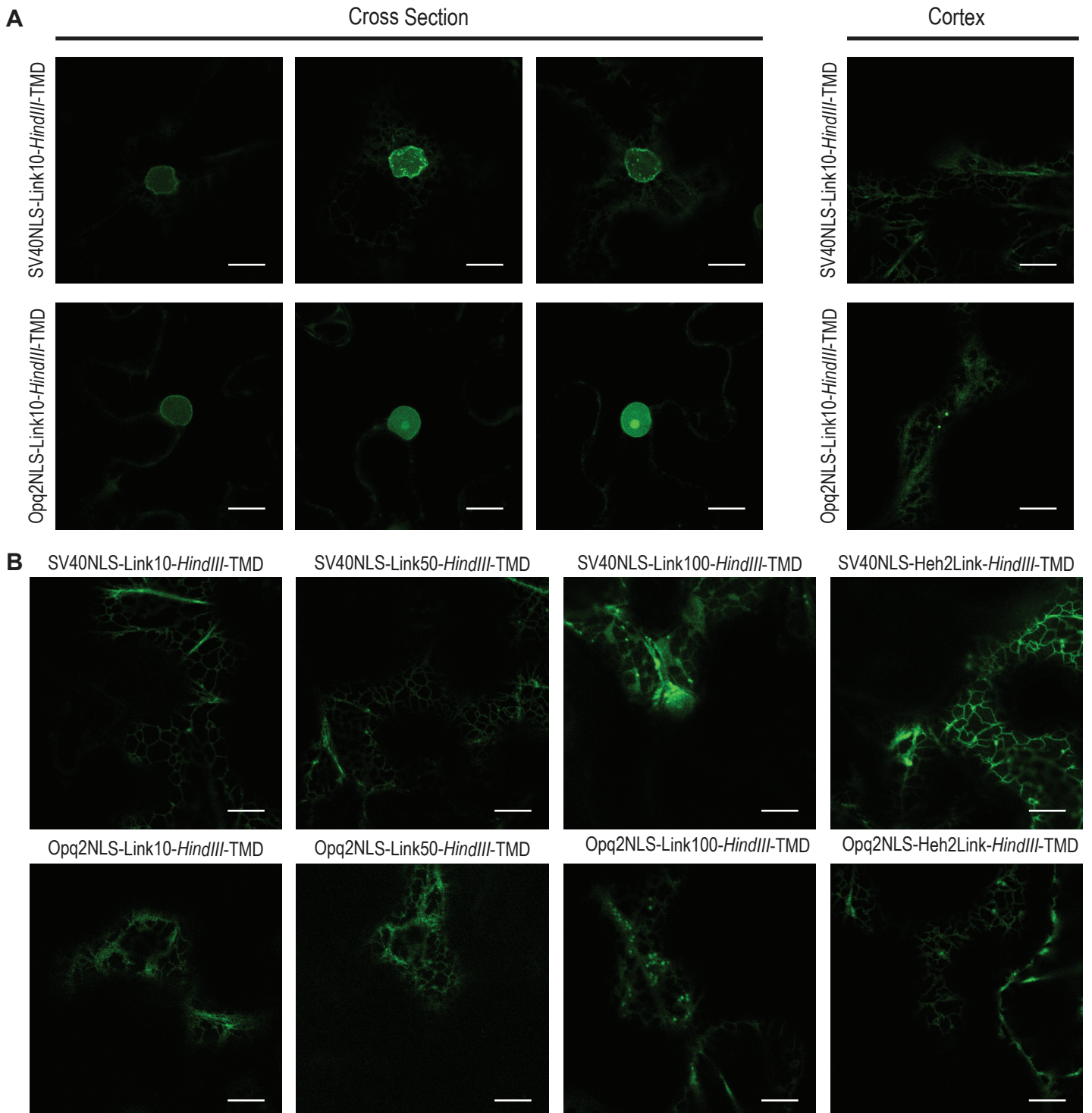


Figure S6. Chimeric membrane proteins with short linkers are associated with the ER.

A. Nuclear cross sections exhibiting increased nuclear fluorescence of chimeric membrane proteins with 10aa linkers between NLS and TMD. Example cortical localization shown on right. Scale bars= 10 μ m **B.** Sample images of cortical localization of chimeric membrane proteins with short linkers. Images were collected at a higher laser power and gain setting to maximize visibility. Scale bars= 10 μ m.

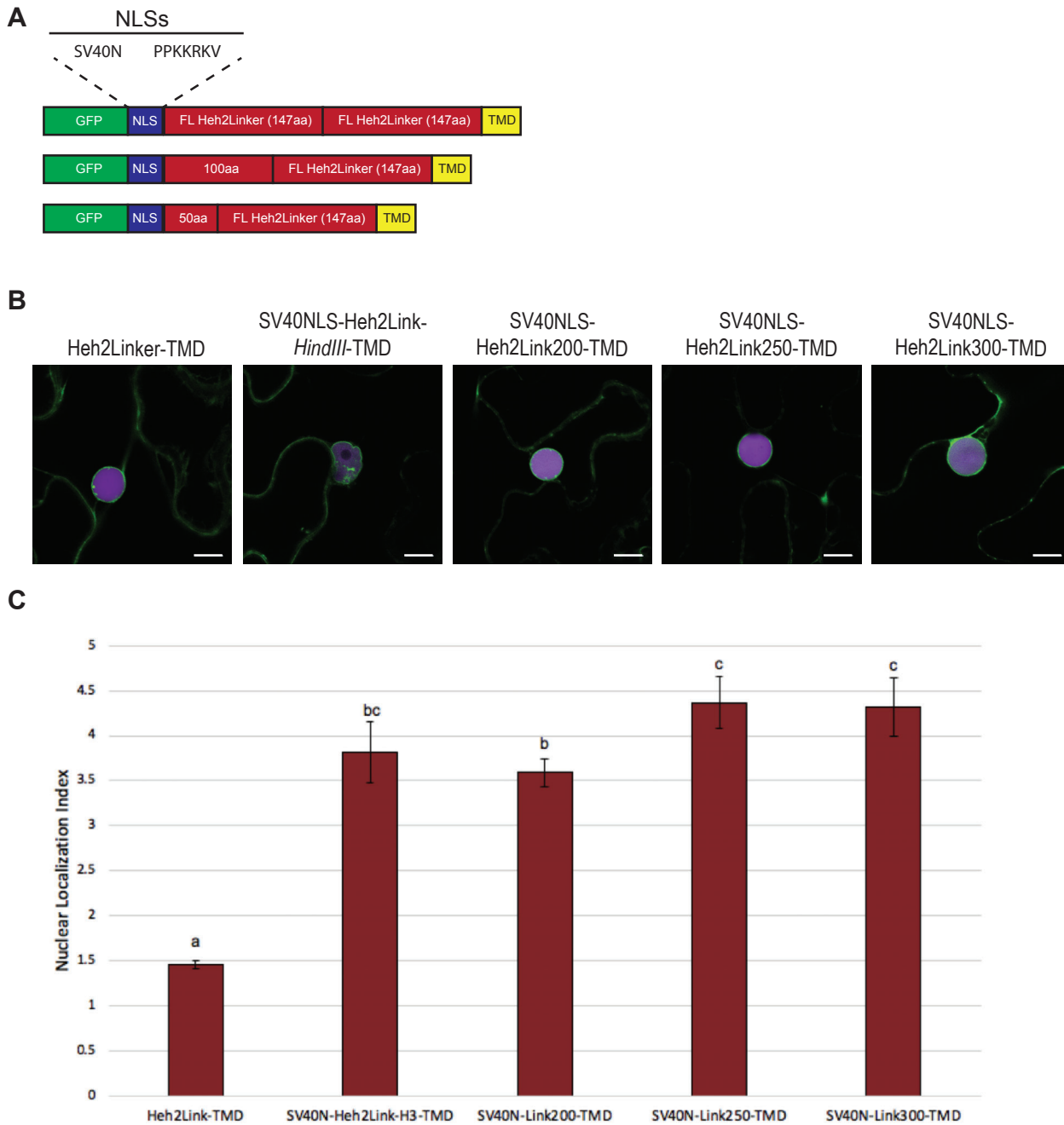


Figure S7. NLS-fused membrane proteins with extralumenal domains exceeding 60kDa are enriched at the nuclear envelope. **A.** A “full length” copy of the Heh2 intrinsically disordered linker was fused to truncations of the Heh2 Linker, resulting in 197, 247 and 297 amino acid linkers between the SV40NLS and TMD. The resulting chimeric proteins had extralumenal domains of 53, 58 and 64kDa, respectively. **B.** The resulting SV40NLS-fused chimeric membrane proteins were transiently co-expressed in *N. benthamiana* leaf epidermal cells with the nuclear marker H2B-mCherry. Scale bars = 10µm. **C.** NLI was calculated for SV40NLS-fused chimeric membrane proteins and a no-NLS control (Heh2Linker-TMD). Statistical groups denoted by letters, where $p < 0.001$ by Student’s T-Test. N between 20-60 cells for all chimeric membrane proteins.

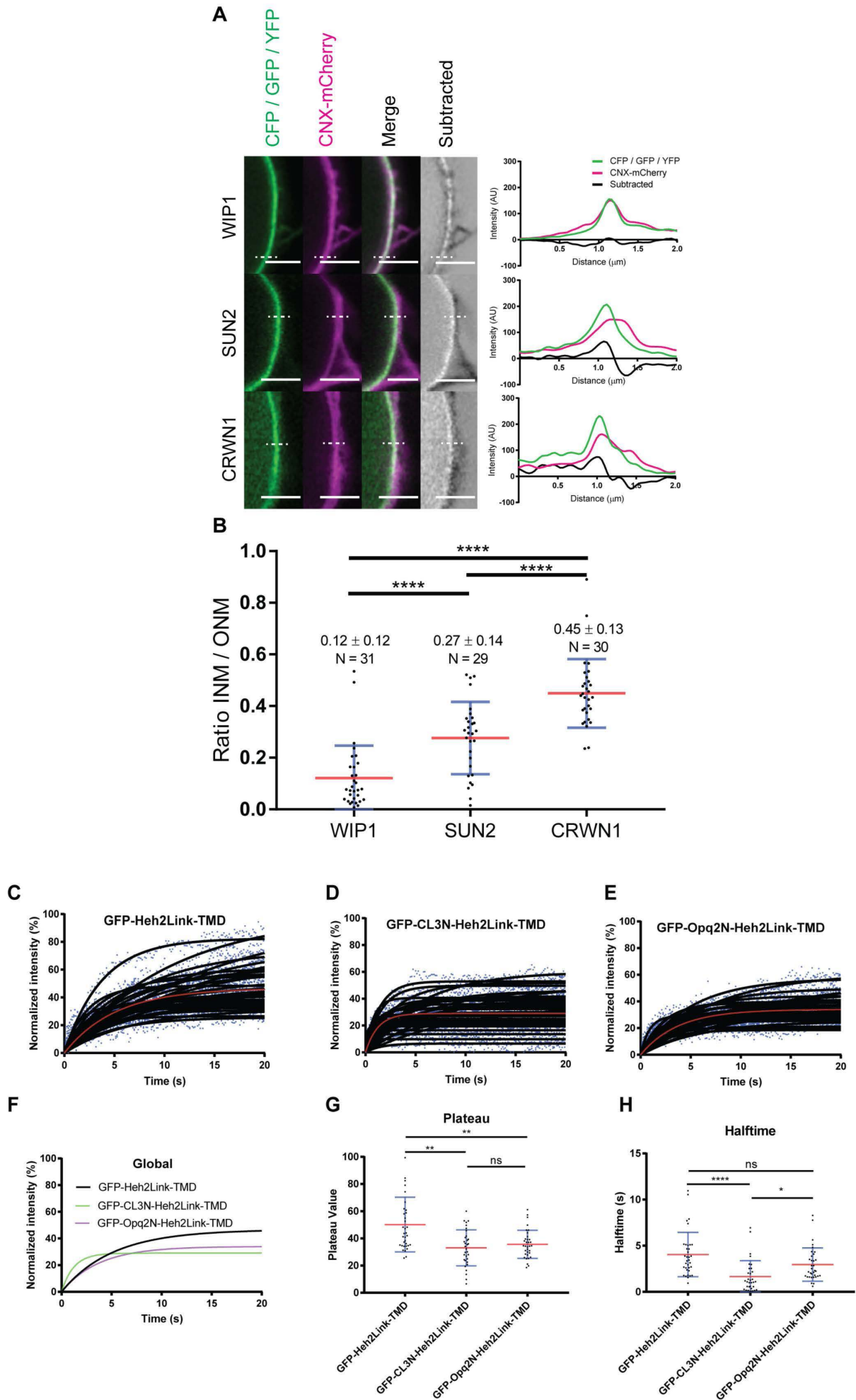


Figure S8. Determining the ratio of INM from ONM fluorescence using Airyscan sub-diffraction limited microscopy and determining mobility of NLS-fused chimeric membrane proteins.

A. Control CNX-mCherry (ONM) fluorescence was subtracted from WIP1 (ONM), SUN2 (INM) or CRWN1 (nuclear periphery) fluorescence. In subtracted images white pixels show positive values, grey and black negative. Representative images shown. Line profiles show CFP / GFP / YFP intensity (green), CNX-mCherry intensity (magenta) and the subtracted signal intensity (black). **B.** Ratio of maximum intensity value of WIP1, SUN2 or CRWN1 over max intensity from the subtracted image. Fluorescence recovery after photobleaching (FRAP) demonstrates that Heh2Link is more mobile than either NLS constructs. **C.** Normalized intensity curves for all repeats of GFP-Heh2Link-TMD FRAP. **D.** Normalized intensity curves for all repeats of GFP-CL3N-Heh2Link-TMD FRAP. **E.** Normalized intensity curves for all repeats of GFP-Opq2N-Heh2Link-TMD FRAP. **F.** Global curves of FRAP for GFP-Heh2Link-TMD, GFP-CL3N-Heh2Link-TMD and GFP-Opq2N-Heh2Link-TMD. **G.** Box plots of plateau values from all FRAP recovery curves in C, D and E. **H.** Box plots of halftime values from all FRAP recovery curves in C, D and E. Scatter dot plot shows mean value in red and error bars (blue) denote standard deviation. Mean \pm standard deviation and N of nuclei quantified shown for each condition. One-way ANOVA statistical test used to test statistical significance. For ANOVA * = $P \leq 0.05$, ** = $P \leq 0.01$, **** = $P \leq 0.0001$ and ns = $P \geq 0.05$.

Table S1. Nuclear localization signals (NLSs) used in this study

Abbreviation	Name	Sequence ^a	Ref
SV40N	SV40 T-Antigen NLS ^b	PP KKKR KV	1
cMycN	cMyc NLS ^b	PAA KRV KLD	2
CL3N	Class 3 NLS ^b	AA AKRS WSAAF	3
CL4N	Class 4 NLS ^b	RPA KRKY FAA	3
CL5N	Class 5 NLS ^b	SVL GKRK F	3
NPN	Nucleoplasmin NLS ^c	KRPAATKRAGQAKKK	4
SUN1N	SUN1 NLS ^c	RTRKVATPKSEKARWKT	5
SUN2N	SUN2 NLS ^c	RTRKSQGNKIDRGKWK	5
Opq2N	Opaque2 NLS ^c	RVKKRKESNRESARRSRYRKA	6

^a Basic amino acid clusters are in bold

^b Monopartite NLSs

^c Bipartite NLSs

¹ Kalderon et al. (1984) Cell

² Dang and Lee (1988) Mol. Cell Biol.

³ Kosugi et al. (2009) J. Biol. Chem.

⁴ Robbins et al. (1991) Cell

⁵ Graumann et al. (2010) Plant J.

⁶ Varagona et al. (1992) Plant Cell

Table S2. Multiple comparisons of statistics for Airyscan Imaging

Control Nuclear Envelope Airyscan co-localization				
Tukey's multiple comparisons test	Mean Diff.	95.00% Confidence Interval of difference	Sign.	P Value
GFP-WIP1 vs. CRWN1-YFP	0.4026	0.3318 to 0.4733	****	<0.0001
GFP-WIP1 vs. SUN2-CFP	0.245	0.1811 to 0.3089	****	<0.0001
CRWN1-YFP vs. SUN2-CFP	-0.1576	-0.2262 to -0.08893	****	<0.0001

PICL Nuclear Envelope Airyscan co-localization				
Tukey's multiple comparisons test	Mean Diff.	95.00% Confidence Interval of difference	Sign.	P Value
GFP-PICL vs. GFP-NLS-PICL	0.1649	0.1041 to 0.2257	****	<0.0001
GFP-PICL vs. GFP-PICL-SIT	0.02654	-0.03423 to 0.08732	ns	0.6742
GFP-PICL vs. GFP-NLS-PICL-SIT	0.06466	0.007164 to 0.1222	*	0.0203
GFP-NLS-PICL vs. GFP-PICL-SIT	-0.1384	-0.208 to -0.06878	****	<0.0001
GFP-NLS-PICL vs. GFP-NLS-PICL-SIT	-0.1003	-0.167 to -0.0335	***	0.0007
GFP-PICL-SIT vs. GFP-NLS-PICL-SIT	0.03812	-0.02864 to 0.1049	ns	0.4558

Artificial Membrane Protein NE Airyscan co-localization				
Tukey's multiple comparisons test	Mean Diff.	95.00% Confidence Interval of difference	Sign.	P Value
GFP-Heh2Link-TMD vs. GFP-CL3N-Heh2Link-TMD	0.4299	0.3666 to 0.4932	****	<0.0001
GFP-Heh2Link-TMD vs. GFP-Opg2N-Heh2Link-TMD	0.1697	0.108 to 0.2314	****	<0.0001
GFP-CL3N-Heh2Link-TMD vs. GFP-Opg2N-Heh2Link-TMD	-0.2602	-0.3189 to -0.2015	****	<0.0001

Significance guide

Sign. = Statistical significance

ns = not significant

* = p≤0.05

*** = p≤0.001

**** = p≤0.0001

Table S3. Primers used in this study

Primer name	GC%	Tm	Sequence (5'-3')	Function
PICLF	41	72	caccATGGAAGAAGCAACAAAAGTGAAGTT	Cloning full length AtPICL from Arabidopsis cDNA
PICLR	25	62.5	TTAATAATTTTTCCCAACAATGATACC	Cloning full length AtPICL from Arabidopsis cDNA
PICLNLSIF	43	78	AAGGTAGAAGACCCCATGGAAGAAGCAACAAAAGTGAAGTT	Fusing the SV40NLS to the N-terminus of AtPICL
PICLNLSIIF	45	81.8	caccATGCCAAAAGAAAGAGAAGGTAGAAGACCCCATGGAAG	Fusing the SV40NLS to the N-terminus of AtPICL
PICLSITR	42	84.1	TCATGTGGGTACAACAGTATCTGGCTCCGGATAATTTTTCCCAACAATGA	Fusing the SIT of AtWIP1 to the C-terminus of AtPICL
ScHeh2F	44	73	ggggacaagttgtacaaaaaagcaggcttATGGATCACAGAAACCTGTATGCCGAAAACCG	Cloning full length ScHeh2 from genomic DNA
ScHeh2R	45	72	ggggaccacttgtacagaagaagctgggtaTATTCTTTCCATCCCAACATG	Cloning full length ScHeh2 from genomic DNA
Heh2NLSF	36	70	ggggacaagttgtacaaaaaagcaggcttATGGTCAAAGATGAAATGTTGAACTAACAAGAG	Cloning NLS-L-TM from ScHeh2
Heh2LinkF	46	73	ggggacaagttgtacaaaaaagcaggcttATGCCACCAGAGTCTCCTCCACAATCTAAG	Cloning Linker and L-TM from ScHeh2
Heh2LinkdStopR	46	71	ggggaccacttgtacagaagaagctgggtaTAACCTACTAGTATCTCCTCTCGTC	Cloning linker and NLS-L from ScHeh2
Heh2TMR	46	73	ggggaccacttgtacagaagaagctgggtaTAGATTAGTTCAGTGTCCAGCTTATCGA	Cloning NLS-L-TM and L-TM from ScHeh2
pKSpeIF	65	70	AGGCGGCCGCACTAGTAGTGG	Modifying pK7WGF2 to introduce SpeI restriction site
pKXbaIR	68	67	CCGGGATCCTCTAGAGGG	Modifying pK7WGF2 to introduce SpeI restriction site
pKpmIIIF	64	86	GATATCCCAGTGGCGGCCCATGCTAGAGTCCG	Modifying pK7WGF2 to introduce PmlI restriction site
pKpmIIR	50	75	CGCACGTGGGATATCACCACCTTTGTACA	Modifying pK7WGF2 to introduce PmlI restriction site
SV40cNLSInFusF	44	67	AGGCGGCCGCACTAGTAGCCACCAAAAAAAGAAAAGTTG	In-fusion cloning of SV40 cNLS into pK7WGF2 Modified Vector
SV40cNLSInFusR	35	64	TGCTCACCATACTAGCAACTTTTCTTTTTTTTTTGGTGCCAT	In-fusion cloning of SV40 cNLS into pK7WGF2 Modified Vector
cMycNLSInFusF	52	72	AGGCGGCCGCACTAGTAGTCCCTGCTGCTAAGAGAGTTAAGCTTGAT	In-Fusion Cloning of cMyc NLS into pK7WGF2 Modified Vector
cMycNLSInFusR	43	68	TGCTCACCATACTAGTAGTCAAGCTTAACTCTCTAGCAGCAGCAT	In-Fusion Cloning of cMyc NLS into pK7WGF2 Modified Vector
Class3NLSInFusF	53	74	AGGCGGCCGCACTAGTAGTGGCTGTGCTAAGAGATCTGTGCTCTGCTGCTTTT	In-Fusion Cloning of Class 3 NLS into pK7WGF2 Modified Vector
Class3NLSInFusR	46	71	TGCTCACCATACTAGTAAAGCAGCAGACCAAGATCTCTTAGCAGCAGCCAT	In-Fusion Cloning of Class 3 NLS into pK7WGF2 Modified Vector
Class4NLSInFusF	49	71	AGGCGGCCGCACTAGTAGACCTGCTAAGAGAAAGTATTTTGGTCT	In-Fusion Cloning of Class 4 NLS into pK7WGF2 Modified Vector
Class4NLSInFusR	40	68	TGCTCACCATACTAGTAGCAGCAAAATCTTCTCTAGCAGGTCTCAT	In-Fusion Cloning of Class 4 NLS into pK7WGF2 Modified Vector
Class5NLSInFusF	47	70	AGGCGGCCGCACTAGTAGTGTCTGTCTTGGAAAGAGAAAGTTGCT	In-Fusion Cloning of Class 5 NLS into pK7WGF2 Modified Vector
Class5NLSInFusR	39	66	TGCTCACCATACTAGTAGCAAACTTCTCTTCCAAGAAGCAGACAT	In-Fusion Cloning of Class 5 NLS into pK7WGF2 Modified Vector
NP-NLSInFusF	55	74	AGGCGGCCGCACTAGTAGAAGAGACCTGCTGCTACTAAGAGAGCTGGACA	In-Fusion cloning of nucleoplasmin NLS into pK7WGF2 Mod. Vector
NP-NLSInFusR	43	69	TGCTCACCATACTAGTCTCTCTCTAGCTTGTCCAGCTCTCTAGTAG	In-Fusion cloning of nucleoplasmin NLS into pK7WGF2 Mod. Vector
SUN1NLSInFusF	62	75	AGGCGGCCGCACTAGTAGCGGACGCGGAAGGTTGCGACTCTAAGTCTGA	In-fusion cloning of SUN1 NLS into pK7WGF2 Modified Vector
SUN1NLSInFusR	53	74	TGCTCACCATACTAGTGTCTTCCACCAGCTTCTCAGACTAGGAGTCTG	In-fusion cloning of SUN1 NLS into pK7WGF2 Modified Vector
SUN2NLSInFusF	57	77	AGGCGGCCGCACTAGTAGCGGACGCGGAAGTCTCAGGGGAATAAGATAGAT	In-fusion cloning of SUN2 NLS into pK7WGF2 Modified Vector
SUN2NLSInFusR	43	70	TGCTCACCATACTAGGTGCTTCCATTTCCCTCTATCTATTTCCCTC	In-fusion cloning of SUN2 NLS into pK7WGF2 Modified Vector
Opq2NLSInFusF	43	71	AGGCGGCCGCACTAGTAGAGTGTAGAAGAGAAAGAACTAATAGAGAATCTGCTAGA	In-Fusion cloning of Opaque 2 NLS into pK7WGF2 Modified Vector
Opq2NLSInFusR	36	61	TGCTCACCATACTAGTGGCTTTCTATATCTAGATCTTACAGAGATCTCTATTAGATT	In-Fusion cloning of Opaque 2 NLS into pK7WGF2 Modified Vector
WIP1TMDInFusF	40	71	GTGGTGAATCCCACAGAGCATGTAAGATCACTCATACGTTCTTATACAGTAGTAGTGTCAACAG	In-fusion cloning of WIP1 TMD into pK7WGF2 Modified Vector
WIP1TMDInFusR	50	78	AGCATGGCCGCGCACCTACTCCGGCAACAATGAGACAGGAGCAACAACTACTGTTGACAGCAATACT	In-fusion cloning of WIP1 TMD into pK7WGF2 Modified Vector
GUSF	42	69	ggggacaagttgtacaaaaaagcaggcttATGTACGCTCTGTAGAA	Gateway cloning of GUS w/o stop codon for NLS/TMD experiments
GUSdeltaStopR	52	74	ggggaccacttgtacagaagaagctgggtaTTGTTGCTCCCTGCTG	Gateway cloning of GUS w/o stop codon for NLS/TMD experiments
GUS693F	55	57	GCAACTGGACAAGGCACTAG	Sequencing GUS
SV40NLSLinklTopoRef	43	71	caccATGCCCAAAAAAAGAAAAGTTccaccagagctctctcca	Cloning Sv40NLS onto ScHeh2 Linker region
CL2NLSLinklTopoF	54	72	caccATGCCTGCTGTAAGAGAGTAAAGCTTGTATccaccagagctctctcca	Cloning cMyc NLS onto ScHeh2 Linker region
CL3NLSLinklTopoF	53	77	caccATGGCTGCTGTAAGAGATCTTGGCTGCTGCTTTTccaccagagctctctcca	Cloning Class 3 NLS onto ScHeh2 Linker region
CL4NLSLinklTopoF	49	74	caccATGAGACCTGCTAAGAGAAAGTATTTGCTGCTccaccagagctctctcca	Cloning Class 4 NLS onto ScHeh2 Linker region
CL5NLSLinklTopoF	48	73	caccATGTCTGTTCTTGGAAAGAGAAAGTTGCTccaccagagctctctcca	Cloning Class 5 NLS onto ScHeh2 Linker region
NPNLSLinklTopoF	51	77	caccATGAAGAGACCTGCTGCTACTAAGAGAGCTGGACAAGCTAAGAGAAAGAAAGccaccagagctctctcca	Cloning Nucleoplasmin NLS onto ScHeh2 Linker region
SUN1NLSLinklTopoF	59	81	CACCATGCGGACGCGGAAGGTTGCGACTCTAAGTCTGAGAAAGCGCGGTGAAGACAccaccagagctctctcca	Cloning SUN1 NLS onto ScHeh2 Linker region
SUN2NLSLinklTopoF	53	78	CACCATGCGGACGCGGAAGTCTCAGGGAATAAGATAGATAGAGGAAAGTGAAGACAccaccagagctctctcca	Cloning SUN2 NLS onto ScHeh2 Linker region
Opq2NLSLinklTopoF	41	73	caccATGAGAGTTAGAAAGAGAAAGAACTTAATAGAGATCTGCTAGAAGATCTAGATATAGAAAGCTccaccagagctctctcca	Cloning Opaque2 NLS onto ScHeh2 Linker region
LinklTopoR	40	55	TAACCTACTAGTATCCTCTCGTCT	Cloning NLSs onto ScHeh2 Linker region (lacking stop codon)
WIP1CCF	41	69	ggggacaagttgtacaaaaaagcaggcttATGATTGTAACCTGGTAAAACAATG	Cloning coiled-coil domain from AtWIP1 into pDONR221
WIP1CCR	44	71	ggggaccacttgtacagaagaagctgggtaTCAGATTCTATGCAATCGTTTTGC	Cloning coiled-coil domain from AtWIP1 into pDONR221
SV40NLSCTTopoF	33	67	caccATGCCCAAAAAAAGAAAAGTTattgtaacctggaacaat	Cloning Sv40NLS onto WIP1 Coiled-Coil Domain
CL2NLSCTTopoF	42	71	caccATGCCTGCTGTAAGAGAGTAAAGCTGATattgtaacctggaacaat	Cloning cMyc NLS onto WIP1 Coiled-Coil Domain
CL3NLSCTTopoF	44	73	caccATGGCTGCTGTAAGAGATCTTGGCTGCTGCTTTattgtaacctggaacaat	Cloning Class 3 NLS onto WIP1 Coiled-Coil Domain
CL4NLSCTTopoF	40	70	caccATGAGACCTGCTAAGAGAAAGTATTTGCTGCTattgtaacctggaacaat	Cloning Class 4 NLS onto WIP1 Coiled-Coil Domain
CL5NLSCTTopoF	33	69	caccATGTCTGTTCTTGGAAAGAGAAAGTTGCTattgtaacctggaacaat	Cloning Class 5 NLS onto WIP1 Coiled-Coil Domain
CTTopoR	40	57	GATTCTATGCAATCGTTTTGCAGG	Cloning NLSs onto WIP1 Coiled-Coil Domain (lacking stop codon)
Heh2Link10H3TopoR	43	62	aagcttTGACTTAGATTGTGGAGGAGACTC	Truncating NLS-Heh2Linker to 10aa (Lacking stop codon)
Heh2Link50H3TopoR	42	62	aagcttCGGCAATCTGGTTTTGGAA	Truncating NLS-Heh2Linker to 50aa (Lacking stop codon)
Heh2Link100H3TopoR	48	63	aagcttTGCTCCAGTTGAAGGACCA	Truncating NLS-Heh2Linker to 100aa (Lacking stop codon)
Heh2LinkH3TopoR	39	60	aagcttTAACCTACTAGTATCCTCTCGTCT	Introducing HindIII restriction site to Heh2 Linker (Lacking stop codon)
Heh2LinkDualH3TopoF	50	69	CACCaaagcttATGCCACCAGAGTCTCCTCCACAATCTAAG	Generating HindIII-Heh2Linker-HindIII for assembling Long Linkers
Heh2LinkDualH3TopoR	30	60	aagcttTAACCTACTAGTATCCTCTCGTCT	Generating HindIII-Heh2Linker-HindIII for assembling Long Linkers
CalnexinTopoF	48	64	caccATGAGACACGGCAACTATTTCCG	Cloning Calnexin into pENTR/D-Topo to generate a C-terminal RFP fusion
CalnexinTopoR	44	59	CTAATTATCAGCTCTCGGTTGCCTT	Cloning Calnexin into pENTR/D-Topo to generate a C-terminal RFP fusion

Table S4. Vectors and primers used in this study

Vector	Antibiotic	Product	Origin	Purpose
pENTR/D-Topo	Kanamycin			Binary Entry vector for use in GATEWAY cloning
pDONR221	Kanamycin			Binary Entry vector for use in GATEWAY cloning
pK7WGF2	Spectinomycin	35SProm::GFP-GW	1	N-terminal GFP-fusion vector
pK7WGF2 Modified	Spectinomycin	35SProm::GFP-GW	This Study	Intermediary for generation of NLS/TMD vectors
pK7TMW0WGF2	Spectinomycin	35SProm::GFP-GW-WIP1TMD	This Study	N-terminal GFP-, C-terminal TMD-fusion vector
pK7WGF1N2	Spectinomycin	35SProm::SV40NLS-GFP-GW	This Study	N-terminal SV40NLS-GFP-fusion vector
pK7WGF2N2	Spectinomycin	35SProm::cMycNLS-GFP-GW	This Study	N-terminal cMycNLS-GFP-fusion vector
pK7WGF3N2	Spectinomycin	35SProm::Class3NLS-GFP-GW	This Study	N-terminal Class3NLS-GFP-fusion vector
pK7WGF4N2	Spectinomycin	35SProm::Class4NLS-GFP-GW	This Study	N-terminal Class4NLS-GFP-fusion vector
pK7WGF5N2	Spectinomycin	35SProm::Class5NLS-GFP-GW	This Study	N-terminal Class5NLS-GFP-fusion vector
pK7WGF6N2	Spectinomycin	35SProm::NP-NLS-GFP-GW	This Study	N-terminal NucleoplasmNLS-GFP-fusion vector
pK7WGF7N2	Spectinomycin	35SProm::SUN1NLS-GFP-GW	This Study	N-terminal SUN1NLS-GFP-fusion vector
pK7WGF8N2	Spectinomycin	35SProm::SUN2NLS-GFP-GW	This Study	N-terminal SUN2NLS-GFP-fusion vector
pK7WGF10N2	Spectinomycin	35SProm::Opq2NLS-GFP-GW	This Study	N-terminal Opaque2NLS-GFP-fusion vector
pK7TMW0WGF1N2	Spectinomycin	35SProm::SV40NLS-GFP-GW-WIP1TMD	This Study	N-terminal SV40NLS-GFP-fusion, C-terminal TMD-fusion vector
pK7TMW0WGF3N2	Spectinomycin	35SProm::CL3NLS-GFP-GW-WIP1TMD	This Study	N-terminal CL3NLS-GFP-fusion, C-terminal TMD-fusion vector
pK7RWG2	Spectinomycin	35SProm::GW-RFP	1	C-terminal RFP-fusion vector
Plasmid	Antibiotic	Product	Origin	Purpose
PICL@pK7WGF2	Spectinomycin	35SProm::GFP-PICL	2	
NLS-PICL@pK7WGF2	Spectinomycin	35SProm::GFP-NLS-PICL	This Study	
PICL-SIT@pK7WGF2	Spectinomycin	35SProm::GFP-PICL-SIT	This Study	
NLS-PICL-SIT@pK7WGF2	Spectinomycin	35SProm::GFP-NLS-PICL-SIT	This Study	
ScHeh2@pK7WGF2	Spectinomycin	35SProm::GFP-ScHeh2	This Study	
Heh2NLS-L-TM@pK7WGF2	Spectinomycin	35SProm::GFP-Heh2NLS-L-TM	This Study	
Heh2L-TM@pK7WGF2	Spectinomycin	35SProm::GFP-Heh2L-TM	This Study	
GUS@pK7WGF2 Modified	Spectinomycin	35SProm::GFP-GUS	This Study	
GUS@pK7WGF1N2	Spectinomycin	35SProm::SV40NLS-GFP-GUS	This Study	
GUS@pK7WGF3N2	Spectinomycin	35SProm::Class3NLS-GFP-GUS	This Study	
GUS@pK7WGF4N2	Spectinomycin	35SProm::Class4NLS-GFP-GUS	This Study	
GUS@pK7WGF5N2	Spectinomycin	35SProm::Class5NLS-GFP-GUS	This Study	
GUS@pK7WGF6N2	Spectinomycin	35SProm::NP-NLS-GFP-GUS	This Study	
GUS@pK7WGF7N2	Spectinomycin	35SProm::SUN1NLS-GFP-GUS	This Study	
GUS@pK7WGF8N2	Spectinomycin	35SProm::SUN2NLS-GFP-GUS	This Study	
GUS@pK7WGF10N2	Spectinomycin	35SProm::Opq2NLS-GFP-GUS	This Study	
Heh2LinkΔStop@pK7TMW0WGF2	Spectinomycin	35SProm::GFP-Heh2Linker-WIP1TMD	This Study	
SV40NLS-Heh2LinkΔStop@pK7TMW0WGF2	Spectinomycin	35SProm::GFP-SV40NLS-Heh2Linker-WIP1TMD	This Study	
cMycNLS-Heh2LinkΔStop@pK7TMW0WGF2	Spectinomycin	35SProm::GFP-cMycNLS-Heh2Linker-WIP1TMD	This Study	
Class3NLS-Heh2LinkΔStop@pK7TMW0WGF2	Spectinomycin	35SProm::GFP-Class3NLS-Heh2Linker-WIP1TMD	This Study	
Class4NLS-Heh2LinkΔStop@pK7TMW0WGF2	Spectinomycin	35SProm::GFP-Class4NLS-Heh2Linker-WIP1TMD	This Study	
Class5NLS-Heh2LinkΔStop@pK7TMW0WGF2	Spectinomycin	35SProm::GFP-Class5NLS-Heh2Linker-WIP1TMD	This Study	
NP-NLS-Heh2LinkΔStop@pK7TMW0WGF2	Spectinomycin	35SProm::GFP-NP-NLS-Heh2Linker-WIP1TMD	This Study	
SUN1NLS-Heh2LinkΔStop@pK7TMW0WGF2	Spectinomycin	35SProm::GFP-SUN1NLS-Heh2Linker-WIP1TMD	This Study	
SUN2NLS-Heh2LinkΔStop@pK7TMW0WGF2	Spectinomycin	35SProm::GFP-SUN2NLS-Heh2Linker-WIP1TMD	This Study	
Opq2NLS-Heh2LinkΔStop@pK7TMW0WGF2	Spectinomycin	35SProm::GFP-Opq2NLS-Heh2Linker-WIP1TMD	This Study	
WIP1CCΔStop@pK7TMW0WGF2	Spectinomycin	35SProm::GFP-WIP1CC-WIP1TMD	This Study	
SV40NLS-WIP1CCΔStop@pK7TMW0WGF2	Spectinomycin	35SProm::GFP-SV40NLSWIP1CC-WIP1TMD	This Study	
cMycNLS-WIP1CCΔStop@pK7TMW0WGF2	Spectinomycin	35SProm::GFP-cMycNLSWIP1CC-WIP1TMD	This Study	
Class3NLS-WIP1CCΔStop@pK7TMW0WGF2	Spectinomycin	35SProm::GFP-Class3NLSWIP1CC-WIP1TMD	This Study	
Class4NLS-WIP1CCΔStop@pK7TMW0WGF2	Spectinomycin	35SProm::GFP-Class4NLSWIP1CC-WIP1TMD	This Study	
Class5NLS-WIP1CCΔStop@pK7TMW0WGF2	Spectinomycin	35SProm::GFP-Class5NLSWIP1CC-WIP1TMD	This Study	
SV40NLS-Heh2Link10-H3@pK7TMW0WGF2	Spectinomycin	35SProm::GFP-SV40NLS-Heh2Link10- <i>HindIII</i> -WIP1TMD	This Study	
SV40NLS-Heh2Link50-H3@pK7TMW0WGF2	Spectinomycin	35SProm::GFP-SV40NLS-Heh2Link50- <i>HindIII</i> -WIP1TMD	This Study	
SV40NLS-Heh2Link100-H3@pK7TMW0WGF2	Spectinomycin	35SProm::GFP-SV40NLS-Heh2Link100- <i>HindIII</i> -WIP1TMD	This Study	
SV40NLS-Heh2Link-H3@pK7TMW0WGF2	Spectinomycin	35SProm::GFP-SV40NLS-Heh2Linker- <i>HindIII</i> -WIP1TMD	This Study	
Opq2NLS-Heh2Link10-H3@pK7TMW0WGF2	Spectinomycin	35SProm::GFP-Opq2NLS-Heh2Link10- <i>HindIII</i> -WIP1TMD	This Study	
Opq2NLS-Heh2Link50-H3@pK7TMW0WGF2	Spectinomycin	35SProm::GFP-Opq2NLS-Heh2Link50- <i>HindIII</i> -WIP1TMD	This Study	
Opq2NLS-Heh2Link100-H3@pK7TMW0WGF2	Spectinomycin	35SProm::GFP-Opq2NLS-Heh2Link100- <i>HindIII</i> -WIP1TMD	This Study	
Opq2NLS-Heh2Link-H3@pK7TMW0WGF2	Spectinomycin	35SProm::GFP-Opq2NLS-Heh2Linker- <i>HindIII</i> -WIP1TMD	This Study	
Heh2LinkΔStop@pK7TMW0WGF1N2	Spectinomycin	35SProm::SV40NLS-GFP-Heh2Linker-WIP1TMD	This Study	
Heh2LinkΔStop@pK7TMW0WGF3N2	Spectinomycin	35SProm::CL3NLS-GFP-Heh2Linker-WIP1TMD	This Study	
CalnexinΔStop@pK7RWG2	Spectinomycin	35SProm::Calnexin-RFP	This Study	
WIP1@pK7WGF2	Spectinomycin	35SProm::GFP-WIP1	3	
SUN2@pB7CWG2	Spectinomycin	35SProm::SUN2-CFP	4	
CRWN1@pEarleyGate101	Spectinomycin	35SProm::YFP-CRWN1	5	
H2B-mCherry	Spectinomycin	35SProm::H2B-mCherry	This Study	

1Karimi et al. (2002) Trends Plant Sci. 7:193

2Venkateshkrishnan et al. (2013) PLOS One 8:357283

3Xu et al. (2007) Plant Cell 17:1157

4Graumann et al. (2010) Plant J 61:134

5Dittmer et al. (2007) Plant Cell 19:2793